Energy Transfer from Wind to Waves

by

Balakumar Balachandran

Thesis submitted to the Faculty of the

Virginia Polytechnic Institute and State University

in partial fulfillment of the requirements for the degree of

Master of Science

in

Aerospace Engineering

APPROVED:

Dr.W.L. Neu, Chairman

Dr.J.A. Schetz

Dr.P. Kaplan

December, 1986

Blacksburg, Virginia

Energy Transfer from Wind to Waves

by

Balakumar Balachandran

Dr.W.L. Neu, Chairman

Aerospace Engineering

(ABSTRACT)

The growth rate function is necessary to determine the energy transfer from wind to waves. Analytically, the growth rate function is determined from the Phillips model, for which the mean velocity profile over water surface is important. The analytical model of Phillips using logarithmic form of the mean velocity profile has not been successful.

In the present study, two different mean velocity profile models have been used. One of them, based on a mixing length formulation, is found to be appropriate. This profile is related to the sea state, through two approaches, thus enabling the growth rate function from analytical model to be linked to the sea state. The growth rate function obtained from the analytical model, using this profile, is found to be comparable to that obtained from empirical relations based on pressure measurements when a correction is made to one of the Phillips coefficients.

Acknowledgements

I sincerely wish to thank Dr. Wayne L. Neu for the advice and encouragement provided during the course of this study. I also wish to thank Dr. J.A. Schetz and Dr. P. Kaplan for serving on my committee.

I would also like to thank my parents for their love and support.

Finally I thank my friends for all their help and encouragement.

Table of Contents

List of Tables

List of Illustrations

NOMENCLATURE

a	wave amplitude
A	linear growth term
A_2	constant
B	exponential growth function
BE	exponential growth term
$\vec{c}$	phase velocity
C	sublayer parameter
C_d	drag coefficient
$\vec{C}_g$	group velocity
$D(\vec{k})$	complex amplitude of a wave component
$E(f)$	point spectrum
$E(f, \theta)$	directional frequency spectrum
f	frequency
$F(\theta)$	spreading function
g	gravitational acceleration
$G_{p\eta}$	cross spectrum of pressure and surface displacement
h_s	roughness length scale

H_{rms}	rms wave height
H_s	significant wave height
$\vec{k}$	wave number
l	mixing length
l_o	wall mixing length
L	fetch
m	significant wave slope parameter
M	correlation coefficient
M_m	correlation coefficient
N	constant
p	wave induced pressure
$\vec{u}$	total velocity
$\vec{U}$	mean velocity
$\vec{U}_p$	wave induced velocity perturbation
$\vec{u'}$	atmospheric turbulent fluctuation
$\vec{u}_*$	friction velocity
$\vec{U}_{5.0}$	wind velocity at 5.0 m above sea surface
$\vec{U}_{10.0}$	wind velocity at 10.0 m above sea surface
U_b	bulk velocity
U_s	slip velocity
S	sum of source functions
S_{in}	energy input from the air
S_{nl}	nonlinear wave-wave interaction
S_{ds}	energy dissipation
t	time
T_m	period corresponding to spectral peak

w	surface velocity in vertical direction
$\vec{x}$	position
z_0	surface roughness
z_m	matched layer height
z_t	transition height
α	angle between wind and wave directions
β	roughness Reynolds number
γ	complex correlation function between pressure and η
δ	displacement of mean streamline
δ_m	thickness of matched layer
δ_u	scaling depth
ζ	significant wave slope
η	surface elevation
θ	direction of propagation
κ	Von Karman's constant
ν	kinematic viscosity
Π	pressure spectrum
ρ, ρ_a	air density
ρ_w	water density
τ_o	wall shear stress
τ_t	turbulent Reynolds stress
τ_w	wave induced Reynolds stress
τ_ν	viscous shear stress
T_τ	total tangential stress
φ	perturbation stream function
Ψ	stream function
ω	radian frequency of a wave

Ω	wave induced vorticity

1. Introduction

In the last few decades, much research has been devoted to increase the knowledge and understanding of the physical mechanisms which govern the generation of wind waves. The knowledge of wave conditions is important for the design of offshore structures, evaluation of ship performance, ship routing, coastal processes and military applications.

Surface waves are primarily caused by wind. One of the earliest explanations for the wind generation of waves was made by Jeffreys (1925). He postulated that the phase difference between the pressure distribution of the air flow and the surface waves created an increase of pressure on the windward side and a decrease of pressure on the leeward side and described it in terms of a sheltering coefficient. Phillips (1957) proposed the resonance model which is based on the resonance between the surface wave modes and the convected pressure fluctuations associated with the turbulent wind blowing over the water surface. Miles (1957) proposed the shear flow model. It considers the perturbation of the mean

shear flow in the air by the disturbed water surface. The air flow is taken to be quasi-laminar in that the mean velocity profile is determined by the turbulent fluctuations, however atmospheric turbulence is neglected by the model. Phillips (1966) extended Miles' analysis to consider the interaction of the wave induced air flow perturbations with the free stream turbulence.

Snyder and Cox (1966), Barnett and Wilkerson (1966) and Moskowitz, Pierson and Mehr (1962,1963,1965) conducted field experiments in which wave growth measurements were made. Snyder and Cox deduced a relation for the growth rate from their experimental results. Inoue (1967) constructed a wave model, in which the growth rate was represented by a curve fit through these observations based on the wave growth measurements. The model later evolved into the Spectral Ocean Wave Model (SOWM), Pierson (1982). The SOWM is being used by the U.S. Navy Fleet Numerical Oceanography Center to forecast ocean wave conditions from predicted winds.

All the experimental measurements made till such time to determine the growth rate of wind waves were based on wave growth measurements. Until recently it was not recognized that the wave growth measurements included nonlinear wave-wave interactions. The JONSWAP experiments of Hasselman et al. (1973) showed the importance of the nonlinear interactions in the evolution of the wave spectrum. Wavetank experiments conducted by Wu et al. (1977,1979) and Plant (1980) have further established the significance of nonlinear wave interactions. A result of these interactions is that the growth of waves whose frequencies are

lower than the dominant frequency is largely due to the energy transfer from the dominant wave region rather than by direct transfer from the wind in many cases.

The energy transfer from the wind to the waves can be determined independently of the nonlinear interaction by measuring the wave induced pressure field above the surface waves or by making measurements of the intial growth of waves whose wavelength is smaller than a certain limit, so that the nonlinear interaction is insignificant. Pressure measurements have been made in the laboratory by Shemdin and Hsu (1967), Shemdin (1969), Wu et al. (1977,1979) and Plant (1980). In the field, pressure measurements have been made by Dobson (1971), Elliot (1972), Snyder (1974) and Snyder et al. (1981). Both wave-follower-mounted probes and fixed probes have been used in the measurements. Larson and Wright (1975) and Kawai (1979) measured the intial growth of waves shorter than 10 centimeters in a wavetank to determine the direct energy transfer from the wind.

The measurements include waves travelling in all directions. Hence the empirical relations, describing the growth rate, based on these measurements are all necessarily in the directionally integrated form. It has been shown (Neu and Kwon, 1985) that, an analytical model should obtain the wind input as a function of the angle between the wind and wave directions. Phillips (1966) developed such an analytical model in terms of the mean velocity profile to determine the wind input. The mean velocity profile was taken to be of logarithmic form and this

model was not successful in determination of the wind input. In this analytical model, the velocity profile is very important in the determination of the wind input.

The mean velocity profile in the boundary layer over land or a solid plane surface has been well established to be of the logarithmic form. But the validity of the logarithmic velocity profile over the free water surface, as opposed to a solid surface, is very much doubted. The mean velocity profile above waves is influenced by waves in the region close to the water surface. Takeda (1963) showed that departures from the logarithmic profile occured close to the sea surface. Neu and Kwon (1985) stress the need for a more appropriate mean velocity profile. In the present study the determination of an appropriate mean velocity profile is attempted.

Velocity profiles which show departures from the logarithmic velocity profile are used to determine the growth rate, using the analytical model of Phillips (1966). The growth rate is compared to that given by the empirical relations based on pressure measurements. Two mean velocity profiles are used, one of which is based on the surface renewal model of Liu et al. (1979) and the other on a mixing length formulation of Rotta (1950) which uses a non-zero wall mixing length. The latter velocity profile is found to be more appropriate.

The sea surface drag coefficient is also associated with the velocity profile. As is the case with the wind energy input to the waves, the drag coefficient has been

determined empirically. Data presentation is usually a correlation of drag coefficient with wind speed at a given height, most commonly ten meters. Intuitively it seems that the drag coefficient should depend on sea state (and thermal stability) as well as wind speed and this is suggested by the scatter in the drag coefficient vs wind speed plots (e.g., Phillips, 1966). Recently Hsu (1985) and Huang et al. (1986) have attempted to model the sea state dependence of the drag coefficient. In the present study, the velocity profile based on the mixing length formulation has been related to the sea state through the wall mixing length. Following Huang et al. (1986), Kitaigorodskii's (1970) roughness length scale is used in the analysis, to relate the drag coefficient to the sea state. Thus the resulting wave growth rate is also related to the sea state through the velocity profile.

Phillips' (1966) analytical model is discussed in the second chapter. The third chapter describes the two mean velocity profiles used in the present study to determine the growth rate. The fourth chapter discusses the numerical evaluation of the growth rate function for the different cases, while the fifth chapter deals with how the growth rate function was related to the sea state.

2. Mechanism of Wave Generation

The theoretical basis used to describe the wave growth is discussed in this chapter.

The energy transfer equation (Hasselman, 1960) describes the evolution of the ocean wave spectrum in deep water in the absence of currents. It reads as

$$\frac{\partial E}{\partial t} + \vec{C}_g \cdot \nabla E = S = S_{in} + S_{nl} - S_{ds} \tag{2.1}$$

where $E(f, \theta; \vec{x}, t)$ is the two-dimensional directional frequency wave spectrum being a function of wave frequency f, propagation direction θ, position $\vec{x}$, and time t. Wave energy propagates with group velocity C_g and is changed by the three source functions on the right-hand side. S_{in}, S_{nl}, *and* S_{ds} represent the wind input, nonlinear wave interaction and dissipation source functions respectively. S is the sum of the three source functions.

The energy input from the wind is represented as

$$S_{in} = A(U, f, \alpha) + B(u_*, f, \alpha)E(f, \theta; \vec{x}, t) \tag{2.2}$$

where U, u_* and α represent the wind velocity, the friction velocity and the angle between the wind and wave directions respectively. The A term representing the energy transfer from the turbulent pressure fluctuations to the wave field is based on the resonance theory of Phillips (1957). It results in a linear growth of the spectrum. The BE term which corresponds to the Miles (1957,1959) theory, represents the the interaction of an already disturbed surface with the wind. It leads to exponential growth of the spectrum.

The A term represents the generation of waves from a calm sea through resonance with the turbulent atmospheric pressure fluctuations. The Phillips (1957) theory can explain the growth of waves only till a certain stage beyond which other mechanisms become dominant. Hasselman (1960) showed that the A function can be represented in terms of the three-dimensional spectrum of the random atmospheric pressure fluctuations $\Pi(\vec{k},\omega)$ as

$$A = \frac{4\pi^2 k\omega^3}{\rho_w^2 g^3}\Pi(\vec{k}, \omega) \tag{2.3}$$

where $\omega = 2\pi f$, k is the magnitude of the wave number $\vec{k} = (k_1, k_2)$, and ρ_w is the density of sea water and g is the gravitational acceleration.

The BE term which represents the linear feedback mechanism is the result of fluctuations induced by sheared wind motion over the surface waves. The earlier models obtained B from empirical relations based on experimental observations. The directional dependence of the B function however cannot be measured. Also a large number of measurements would be required to obtain B as a function of the sea state. The directional dependence of the B function and its relation to the sea state, can be determined by means of an analytical model. It is necessary to consider improvements on the present analytical models to obtain a better description of the B function. In the following paragraphs Phillips' (1966) analytical model is described.

A cartesian co-ordinate system as shown in Figure 1 is used. The x axis points in the direction of wave propagation and the z axis points vertically upward. A frame of reference moving with the wave speed c is considered. In the moving frame of reference, the total velocity of the air flow is given by

$$\vec{u} = \vec{U}(z) + \vec{U}_p(x,z) + \vec{u}'(x,y,z,t) - \vec{c} \tag{2.4}$$

where $\vec{U}$ is the mean velocity, $\vec{U}_p = (U_p, V_p, W_p)$ is the wave induced velocity perturbation and $\vec{u}'$ is the random atmospheric turbulent fluctuation. The y-average of the velocity field $\vec{u}$, $<\vec{u}>$ is

$$<\vec{u}> = \vec{U}(z) + \vec{U}_p(x,z) - \vec{c} \tag{2.5}$$

Assuming incompressibility, i.e. $\nabla \cdot <\vec{u}> = 0$, the stream function Ψ , can be defined as

$$\frac{\partial \Psi}{\partial x} = - W_p$$

$$\frac{\partial \Psi}{\partial z} = U \cos \alpha - c + U_p \tag{2.6}$$

Since U_p and W_p are periodic in the x direction, the streamline of the mean motion has the form of the real part of

$$\Psi = \int_{z_m}^{z} \{U(\xi) \cos \alpha - c\} d\xi + \varphi(z) e^{ikx} = const. \tag{2.7}$$

where z_m stands for the matched layer height. The real part of φ, the perturbation stream function, following Phillips (1966) is taken as

$$Re\{\varphi(z) e^{ikx}\} = - k^{-1} \tilde{W}_p(z) \cos[kx + \varepsilon(z)] \tag{2.8}$$

where $\tilde{W}_p(z)$ is the amplitude of $W_p(z)$ and Re means the real part.

The matched layer height, z_m, is the height at which the component of the mean wind velocity in the wave direction matches the phase velocity of the wave. In the frame of reference moving with the wave, the mean streamlines in the matched layer region form closed loops centered on z_m . Figure 1 shows the streamlines in the flow as seen in the moving frame of reference. At the matched

layer, using a Taylor series expansion to represent U(z), equation (2.7) can be approximated to represent the streamlines as

$$\Psi = \frac{1}{2}(z - z_m)^2 U'(z_m) \cos\alpha - \frac{\tilde{W}_p(z) \cos[kx + \varepsilon(z)]}{k} \tag{2.9}$$

Away from the matched layer the mean streamlines undulate about their mean levels z_1. The displacement of the mean streamlines about their average height z_1 can be obtained using equations (2.7) and (2.8) as

$$\delta = \frac{\tilde{W}_p(z_1) \cos[kx + \varepsilon(z)]}{k[U(z_1) \cos\alpha - c]} \tag{2.10}$$

The thickness δ_m of the matched layer can be obtained using equation (2.9) as

$$\delta_m = \{\frac{4\tilde{W}_p(z_m)}{kU'(z_m) \cos\alpha}\}^{\frac{1}{2}} \tag{2.11}$$

The momentum equation is averaged over the x-direction and the y-direction to give the mean stress balance as

$$\frac{\partial}{\partial x_j}\overline{U_{pi}U_{pj}} + \frac{\partial}{\partial x_j}\overline{u'_i u'_j} = -\frac{1}{\rho}\frac{\partial \bar{p}}{\partial x_i} + \nu\frac{\partial^2 U_i}{\partial x_j^2} \tag{2.12}$$

where ρ is the air density, ν is the kinematic viscosity of air and $\bar{p}$ is the pressure averaged over x and y directions. The component of equation (2.12) in the x-direction is

$$\frac{\partial}{\partial z}\{\overline{U_p W_p} + \overline{u'w'} - \nu \frac{\partial}{\partial z}(U \cos \alpha)\} = 0. \tag{2.13}$$

The above equation means that the total tangential stress T_τ is constant with height in the air above water. This is represented by

$$T_\tau = \tau_w + \tau_t + \tau_\nu = const. \tag{2.14}$$

where τ_w , τ_t , τ_ν represent the wave induced Reynolds stress, the turbulent Reynolds stress and the viscous stress respectively. The second and third terms on the right-hand side of the above equation appear in the turbulent flow of a viscous fluid. In an inviscid flow both these terms drop out. Phillips (1966) showed that the following equation is a sufficient approximation to determine the momentum flux to the waves even for a turbulent flow.

$$T_\tau = \tau_w(0) \tag{2.15}$$

where $\tau_w(0)$ is the wave induced Reynolds stress at the surface.

Bryant (1966) showed that τ_w is related to the average of the product of the wave induced vorticity, Ω, and the vertical component of the wave induced velocity perturbation, W_p , as

$$\tau_w(0) = \rho \int_o^\infty \overline{\Omega W_p}\, dz \tag{2.16}$$

The basic flow has a mean vorticity distribution U'(z) cosα. The wave induced vorticity produces variations from the mean vorticity distribution of the turbulent

air flow. This variation from the mean vorticity is proportional to the mean velocity gradient and the magnitude of the undulations of the mean streamlines. It is as

$$|\Omega| \propto |U''(z)\delta \cos \alpha| \tag{2.17}$$

Using equations (2.10), (2.11) and (2.17), an expression for $\overline{\Omega W_p}$ is formed. Outside the matched layer, we have

$$\overline{\Omega W_p} = - M \frac{U''(z)\overline{W_p^2(z)} \cos \alpha}{k|U(z) \cos \alpha - c|} \tag{2.18}$$

while in the matched layer, we have

$$(\overline{\Omega W_p})_m = - M_m U''(z_m) W_p(z_m) \delta_m \cos \alpha \tag{2.19}$$

where M and M_m are correlation coefficients.

In inviscid flow, $\overline{\Omega W_p} = 0$ outside the matched layer since Ω and W_p are in exact quadrature. In turbulent flow, due to diffusion it is possible for a non-zero correlation to exist between them and hence a non-zero M.

Combining equations (2.16) and (2.19), the contribution to the wave induced Reynolds stress across the matched layer is

$$\tau_w|_m = M_m \rho (\overline{\Omega W_p})_m \delta_m$$

$$= - M_m \rho U''(z_m) W_p(z_m) \delta_m^2 \cos \alpha$$

$$= M_m \rho \{ \frac{- U'' \overline{W}_p^2}{kU'} \}_{z_m} \tag{2.20}$$

The equation (2.20) was originally derived by Miles (1957). The total wave induced Reynolds stress at z = 0 is given by combining equations (2.16), (2.18) and (2.20) as

$$\tau_w(0) = M_m \rho \{ \frac{(- U'') \overline{W}_p^2}{kU'} \}_{z_m} + M \rho \int_o^\infty \frac{(- U'') \overline{W}_p^2 \cos \alpha}{k | U \cos \alpha - c |} dz \tag{2.21}$$

where the matched layer should be excluded from the range of the integral. The expressions for W_p as given in Phillips' (1966) model are given below. They are based on the analysis of Miles (1957).

Outside the matched layer

$$W_p = - iNka \{ U(z) \cos \alpha - c \} e^{-kz} e^{ikx} \tag{2.22}$$

where N is a constant. Inside the matched layer

$$W_p = \frac{- iNak^3 e^{ikx}}{U'(z_m) \cos \alpha} \int_{z_m}^\infty \{ U(z) \cos \alpha - c \}^2 e^{-kz} dz \tag{2.23}$$

The wave induced Reynolds stress at the surface is related to B as shown in the next equation.

$$\frac{B}{f} = \frac{2\tau_w(0)}{\rho_w c^2 k^2 a^2} \tag{2.24}$$

where a is the wave amplitude. From equations (2.21), (2.22), (2.23) and (2.24)

$$\frac{B}{f} = \frac{\rho_a}{\rho_w}\frac{1}{c^2 k}\{\frac{M_m N^2 k^4}{\cos^2\alpha}(\frac{-U''}{(U')^3})_{z_m}(\int_{z_m}^{\infty}[U(z)\cos\alpha - c]^2 e^{-kz}dz)^2$$

$$+ M\int_o^{\infty} N^2(-U'')\cos\alpha\,|U\cos\alpha - c|\,e^{-2kz}dz\} \tag{2.25}$$

where ρ_a has been used for the air density ρ. The values suggested by Phillips for the coefficients and constants are $M_m = \pi$, $M = 1.6 \times 10^{-2}$, $N^2 = \frac{1}{3}$ for $z > z_m$ and $N^2 = 1$ for $z < z_m$. From equation (2.25) it is evident that the mean velocity profile is very important in the determination of B/f. The two velocity profiles described in the next chapter are used to determine B/f using the equation (2.25).

Kwon (1986) used the logarithmic velocity profile and the Gauss-Laguerre quadrature scheme to evaluate the integrals in equation (2.25). He adjusted the constants M and M_m in his study to obtain a B/f *vs* u_*/c curve which was similar to Inoue's (1967) curve. In the present study the focus is on the determination of an appropriate mean velocity profile for the evaluation of B/f values. A correction to the correlation coefficient M is found necessary in this study.

At this stage, a discussion of the two types of B function is in order. The empirical relations based on experimental observations, which are used to determine B

can be distinguished into two groups, one based on the wave growth measurements and the other on the pressure measurements. The wave growth measurements made by Snyder and Cox (1966), Barnett and Wilkerson (1966), Moskowitz, Pierson and Mehr (1962,1963,1965) and the curve fit to this data made by Inoue (1967) to represent the B function include the effects of both the wind input, S_{in} and the nonlinear wave interaction, S_{nl} source functions while the measurements based on pressure fluctuations as in the case of Snyder et al. (1981), Plant (1982) and Hsiao and Shemdin (1983) include only the S_{in} source function. Figure 2 shows two curves, one of them being Inoue's curve fit which is based on the wave growth measurements and the other being Snyder's empirical relation which is based on the pressure measurements. The velocity profile based on mixing length formulation is used for Snyder's curve. The wind speed at 10 m height is 15.00 m/s and wall mixing length is $2.314 \cdot 10^{-4}$ m for this profile. At the lower values of $\frac{u_*}{c}$, a significant difference between the two curves can be seen in the figure. The difference between the curves is due to the nonlinear wave interaction, which transfers energy generally from higher to lower frequency waves, being attributed to the wind energy input in Inoue's curve.

The nonlinear wave interaction represented by the source function S_{nl} is described by an analytical relation (Hasselman, 1961). Thus for wave models using a pressure measurement based B function, the S_{nl} source function is included explicitly while those using a growth measurement based B function do not include S_{nl} since it is treated implicitly in the S_{in} source function. It has been recognized,

SWAMP group (1985), that explicit inclusion of S_{nl} is necessary to model observed wave generation.

The dissipation source function, S_{ds}, is incorporated implicitly in most wind wave models through a mechanism which prevents the wave spectrum from exceeding a prescribed fully developed limit. It becomes effective when the spectrum approaches the fully developed limit which is usually taken to be the Pierson-Moskowitz (1964) spectrum (refer Kwon, 1986). Komen et al. (1984) proposed an expression for the dissipation source function for use in numerical wave models. Wave breaking, viscous effects and in some cases, bottom friction are the mechanisms of dissipation. Wave breaking is considered to be a primary mechanism of dissipation.

3. Velocity Profile Models

Two mean velocity profile models have been used in the present study to determine the growth rate. The first model (profile 1) is based on the surface renewal model of Liu et al. (1979) to describe the velocity profile in the region close to the air-sea interface. This region is called the interfacial sublayer. Beyond the sublayer the profile is logarithmic in nature. The second model (profile 2) is based on a mixing length formulation. Rotta's (1950) formulation of the mixing length for a fully rough surface has been used. Both the profiles differ significantly from the logarithmic velocity profile in the region close to the surface. The two velocity profiles are derived and discussed in the following sections.

3.1 Profile 1

Liu et al. (1975,1979) proposed the surface renewal model in their study on air-sea exchanges of heat and water vapor. The model is based on the assumption

that the fluid in contact with the interface becomes unstable and is intermittantly replaced by the fluid from the bulk. According to Liu et al., the momentum transport in the vicinity of a smooth surface can be defined by the following relation.

$$\frac{(U - U_s)}{(U_b - U_s)} = (1 - e^{-\frac{z}{\delta_u}}) \tag{3.1}$$

where U_s is the slip velocity, U_b is the bulk velocity and δ_u is a scaling depth equivalent to the thickness of a laminar layer in which the velocity varies linearly from U_s at the surface to U_b across its depth. In the present study U_s is taken to be zero. The scaling depth is defined as

$$\delta_u = \frac{\rho \nu U_b}{\tau_o} \tag{3.2}$$

where τ_o is the wall shear stress. A sublayer parameter C is defined as

$$C = \frac{U_b}{u_*} \tag{3.3}$$

Using equations (3.1) and (3.3), with $U_s = 0$ we get

$$U = u_* C(1 - e^{-\frac{z}{\delta_u}}) \tag{3.4}$$

The above equations hold in the sub-layer. The sub-layer thickness, also called the transition height is represented by z_t.

The logarithmic velocity profile holds above the transition height. The velocity profile is defined as

$$U(z) = u_* C(1 - e^{-\frac{z}{\delta_u}}) \qquad z \leq z_t$$

$$U(z) = \frac{u_*}{\kappa} \ln(\frac{z}{z_0}) \qquad z \geq z_t \tag{3.5}$$

where κ is Von Karman's constant and z_0 is the roughness length. The slope and the magnitude of the sublayer profile and the logarithmic velocity profile are matched at the transition height to ensure smooth transition. This gives two more relations as below.

$$C(1 - e^{-\frac{z_t}{\delta_u}}) = \frac{\ln(\frac{z_t}{z_0})}{\kappa} \tag{3.6}$$

$$\frac{C}{\delta_u} e^{-\frac{z_t}{\delta_u}} = \frac{1}{\kappa z_t} \tag{3.7}$$

The surface roughness z_0 is a fictitious length scale whose definition depends on the nature of the surface. The surface roughness of a smooth sea surface has the following functional form (e.g., Kondo, 1975; Liu et al., 1979).

$$z_0 = \frac{\beta \nu}{u_*} \tag{3.8}$$

where β is a constant equal to 0.11. For a rough sea surface, the form proposed by Charnock (1955) on dimensional grounds, is

$$z_0 = d\frac{u_*^2}{g} \tag{3.9}$$

where d is a constant which has a value of 0.0112 (Wu 1968). There are also other formulations used to characterise the sea surface roughness (e.g., Kitaigorodskii, 1970 and Hsu, 1974). McDonald (1982) hypothesised that the departure from the logarithmic velocity profile occurs in a manner similar to that proposed by Liu et al. (1979), even for a rough surface. To extend the analysis to rough surfaces, he proposed the following form for the surface roughness z_0.

$$z_0 = \frac{0.11\nu}{u_*} + \frac{0.01u_*^2}{g} \tag{3.10}$$

However, he left δ_u as defined for the smooth surface by equation (3.2).

In the present study a relation between the two fictitious length scales, the scaling depth and the surface roughness has been assumed, on dimensional grounds as

$$\delta_u = CA_2 z_0 \tag{3.11}$$

where A_2 is a constant. The above equation is a general relation which can be used for smooth and rough surfaces. This equation replaces equation (3.2). For a smooth surface, the above equation reduces to equation (3.2) when the surface roughness is defined by equation (3.8) and A_2 is given the value of $1/\beta$.

A system of equations as shown below can be obtained.

$$z_0 = f(\frac{\nu}{u_*}, \frac{u_*^2}{g})$$

$$\delta_u = \frac{z_t \ln(\frac{z_t}{z_0})}{e^{\frac{z_t}{\delta_u}} - 1}$$

$$C = \frac{\delta_u}{\kappa z_t} e^{\frac{z_t}{\delta_u}}$$

$$\delta_u = C A_2 z_0 \tag{3.12}$$

The first equation states the general functional form of the surface roughness. The second and third equations are obtained using equations, (3.6) and (3.7). The fourth equation is equation (3.11). Using the last three equations for a given A_2, the values of C, $\frac{z_t}{z_0}$ and $\frac{\delta_u}{z_0}$ are determined. If the form of surface roughness is known then the other related quantities can be determined.

When, the functional form of the surface roughness is defined by equation (3.8) with $\beta = 0.11$ and A_2 is taken to be 9.09, Liu et al.'s velocity profile is obtained. The surface roughness taken as in equation (3.10) and $A_2 = 9.09$ gives the velocity profile shown in the McDonald (1982) paper. In this study, the surface is assumed to be fully rough and the surface roughness is taken in the form specified by equation (3.9). Figure 3 shows how the velocity profiles vary as A_2 is varied. The wind speed at 10 m height is 15.00 m/s for all three profiles shown in the

figure. As A_2, is increased the transition height increases thus extending the interfacial sublayer. The different profiles merge into the logarithmic velocity profile, as seen in Figure 3. The values of B/f are determined using the analytical model described in the second chapter, for each of these velocity profiles.

3.2 Profile 2

The total shear stress at any location in a turbulent flow can be expressed by the following relation.

$$\tau = \rho\nu \frac{dU}{dz} + \rho\, l^2 \left(\frac{dU}{dz}\right)^2 \tag{3.13}$$

where the first term represents the viscous shear stress and the second term represents the turbulent shear stress. The turbulent shear stress, τ_t, is based on the Prandtl mixing length theory where l is the mixing length (e.g., Schetz, 1984). In a laminar flow only the first term exists.

If the longitudinal pressure gradient is zero, then the total shear stress τ is approximately equal to the wall shear stress τ_o close to the wall. Using $u_*^2 = \tau_o/\rho$ and equation (3.13) the following equation is obtained.

$$l^{+2} \left(\frac{dU^+}{dz^+}\right)^2 + \frac{dU^+}{dz^+} = 1 \tag{3.14}$$

where l^+, U^+ and z^+ are non-dimensional quantities defined as below.

$$l^+ = \frac{u_* l}{\nu}$$

$$z^+ = \frac{u_* z}{\nu}$$

$$U^+ = \frac{U}{u_*} \tag{3.15}$$

Equation (3.14) is a quadratic equation in $\frac{dU^+}{dz^+}$. It is solved for $\frac{dU^+}{dz^+}$ and then integrated from the wall where $U^+ = 0$ and $z^+ = 0$ to obtain the following relation for the mean velocity profile.

$$U^+ = \int_o^{z^+} \frac{2}{1 + \sqrt{1 + 4l^{+2}}} dz^+ \tag{3.16}$$

The form of mixing length assumed decides the velocity profile, as is evident from the above relation. In the present study the sea surface is assumed to be a fully rough surface. Following Granville (1985), the Rotta (1950) formulation for a fully rough surface is used. The mixing length l at a distance z from the surface is represented as

$$l = l_o + \kappa z \tag{3.17}$$

where l_o is the wall mixing length.

The mixing length l, an eddy scale-length, is taken as some effective interaction distance between eddies (e.g., Schetz, 1984). The formulation (3.17) envisages a

decreasing diameter of eddies as the surface is approached. The diameter of the eddies does not go to zero at the wall in this formulation. The non-zero wall mixing length means that the eddies don't die out at the surface and is considered to represent the nature of the free surface. Using equation (3.17) in equation (3.16) and carrying out the necessary integration the following velocity profile is obtained.

$$U^+ = \frac{1}{\kappa}\{\frac{0.5 - \sqrt{l^{+2} + 0.25}}{l^+} - \frac{0.5 - \sqrt{l_o^{+2} + 0.25}}{l_o^+} + \ln(\frac{l^+ + \sqrt{l^{+2} + 0.25}}{l_o^+ + \sqrt{l_o^{+2} + 0.25}})\} \tag{3.18}$$

If the wall mixing length is zero, i.e. $l = \kappa z$, integration of equation (3.16) yields a logarithmic velocity profile. At higher values of z equation (3.18) approaches the logarithmic form shown below.

$$U^+ = \frac{1}{\kappa} \ln z^+ + B_1 \tag{3.19}$$

where B_1 is given by

$$B_1 = \frac{1}{\kappa}\{\ln(4\kappa) - 1 - \frac{0.5 - \sqrt{l_o^{+2} + 0.25}}{l_o^+} - \ln(2l_o^+ + 2\sqrt{l_o^{+2} + 0.25})\} \tag{3.20}$$

Equation (3.18) represents the velocity profile obtained from the mixing length formulation. Unlike the logarithmic velocity profile, this profile doesn't have a

singularity at the surface and this results in a significant difference between the two velocity profiles, close to the surface. The specification of any two of the friction velocity, the mean velocity at a given height or the wall mixing length defines the mean velocity profile. Figure 4 shows how the profiles vary for different values of the wall mixing length. For the three wall mixing lengths shown in the figure, the friction velocity is chosen in each case such that the mean velocity at 10 m height is 15.00 m/s. In the present study the wall mixing length has been related to the sea state through the drag coefficient. When this velocity profile is used to determine the B/f values, the values are found to compare with the values given by the empirical relations based on pressure measurements.

4. Evaluation of the B function

The directionally integrated form of the energy transfer equation is derived in this chapter. The scheme used to evaluate the B/f values is discussed and the results obtained are presented. The B function obtained from measurements of wave induced pressure fluctuations is in directionally integrated form. In order to compare the B function obtained from the analytical model with that obtained from empirical relations the directionally integrated form of the analytical B function is necessary. The following paragraph describes how the B function is found from measurements of wave induced pressure fluctuations, following Plant (1982). This is followed by a discussion of the directional integration necessary for comparison. Finally, the directional behavior of the B function is examined.

The wave induced pressure p on the surface of a wave field can be written as

$$p = \int P(\vec{k})\, e^{i\vec{k}\cdot(\vec{x} - \vec{c}\,t)}\, d\vec{k} \tag{4.1}$$

where $P(\vec{k})$ is the amplitude of the pressure field component with wave-number $\vec{k}$. It is expressed as

$$P(\vec{k}) = \rho_a c^2 k \gamma D(\vec{k}) \tag{4.2}$$

where γ is a complex dimensionless function of frequency, direction and wind speed and $D(\vec{k})$ is the complex amplitude of a wave component. The surface elevation η is defined as

$$\eta(\vec{x}, t) = \int D(\vec{k}) e^{i\vec{k} \cdot (\vec{x} - \vec{c}\, t)} d\vec{k} \tag{4.3}$$

Assuming deep water, we have the following relation.

$$c\omega = g \tag{4.4}$$

where ω is the radian frequency of the wave having phase speed c. Equation (4.3) is used to obtain the surface velocity w in the vertical direction.

$$w = \frac{\partial \eta}{\partial t} = - \int i\omega D(\vec{k}) e^{i\vec{k} \cdot (\vec{x} - \vec{c}\, t)} d\vec{k} \tag{4.5}$$

The rate of work done by atmospheric pressure on the wave field can be written as

$$\rho_w g \int \frac{\partial E(\vec{k})}{\partial t} d\vec{k} = - Re\, \overline{(p^* w)} \tag{4.6}$$

where p^* is the complex conjugate of wave induced pressure p (superscript * means the complex conjugate and bar indicates an average in x and y directions at an instant t) and $E(\vec{k})$ is the wave number spectrum. Equations (4.1) and (4.5) can be used to obtain the following equation.

$$-\overline{Re(p^* w)} = Re\{\int\int \overline{i\omega P^*(\vec{k})\, D(\vec{k}_1)} e^{-i\vec{k}\cdot(\vec{x}-\vec{c}\,t)}\, e^{i\vec{k}_1\cdot(\vec{x}-\vec{c}\,t)} d\vec{k}\; d\vec{k}_1\} \tag{4.7}$$

Using equation (4.2) and the following relation (refer appendix) in equation (4.7)

$$\overline{D^*(\vec{k})D(\vec{k}_1)} = \delta(\vec{k}-\vec{k}_1)E(k) \tag{4.8}$$

we get

$$-\overline{Re(p^* w)} = Re\{\int i\omega\rho_a g\gamma^* E(k) d\vec{k}\} \tag{4.9}$$

Comparing equation (4.9) with equation (4.6) we get

$$\frac{\partial E(\vec{k})}{\partial t} = \left(\frac{\rho_a}{\rho_w}\right)\omega\, Im\gamma\, E(\vec{k}) \tag{4.10}$$

where *Im* refers to the imaginary part. In the above discussion $E(\vec{k})$ is used for notational convenience to represent the two dimensional spectrum $E(f, \alpha)$. Assuming, the wave field to be sufficiently developed, the A term can be neglected compared to the BE term (refer equations 2.1 and 2.2) and the B function can be found from equation (4.10) as

$$B(f, \alpha) = \frac{1}{E(f, \alpha)} \frac{\partial E(f, \alpha)}{\partial t} = (\frac{\rho_a}{\rho_w}) \omega \, Im\gamma \tag{4.11}$$

With a single pressure transducer and wave staff the one dimensional transform of the covariance of pressure and wave height $G_{p\eta}$ is measured (e.g., Snyder et al., 1981). It is expressed in terms of E and γ as

$$G_{p\eta} = \rho_a \int_{-\pi/2}^{+\pi/2} c \, \omega \, \gamma^* \, E(f, \alpha) \, d\alpha \tag{4.12}$$

The normal assumptions of directional dependence are

$$B(f, \alpha) = B(f) \cos \alpha \tag{4.13}$$

and

$$E(f, \alpha) = E(f)[\frac{2 \cos^2 \alpha}{\pi}] \qquad |\alpha| < \frac{\pi}{2} \tag{4.14}$$

Multiplying equation (4.11) by $E(f, \alpha)$ on both sides and using equations (4.13) and (4.14) one can obtain

$$B(f) (\frac{2 \cos^3 \alpha}{\pi}) = \frac{\rho_a \, c \, \omega \, Im\gamma \, E(f, \alpha)}{\rho_w \, c \, E(f)} \tag{4.15}$$

Integrating equation (4.15) with respect to α between the limits $-\frac{\pi}{2}$ and $\frac{\pi}{2}$ and using equation (4.12) we get

$$B(f) = (\frac{3\pi}{8}) \frac{ImG^{*}_{p\eta}}{\rho_w c E(f)} \tag{4.16}$$

Equation (4.16) is the directionally integrated form of the B function obtained from pressure measurements. In the above formulation $B(f) = B(f, 0)$ (refer equation 4.13). This is made use of in determining $B(f)$ from the empirical relations.

The empirical relations based on pressure measurements are as below. They all have assumed directional dependence. Snyder et al.'s (1981) relation is

$$\frac{B}{f} = 0.25\frac{\rho_a}{\rho_w} 2\pi(\frac{U_5 \cos\alpha}{c} - 1) \qquad (\frac{U_5 \cos\alpha}{c}) > 1.0$$

$$\frac{B}{f} = 0.0 \qquad (\frac{U_5 \cos\alpha}{c}) \leq 1.0 \tag{4.17}$$

where U_5 stands for the wind speed at the height of five meters. Plant's (1982) relation is

$$\frac{B}{f} = 0.04(\frac{u_*}{c})^2 2\pi \cos\alpha \qquad f \geq \frac{g}{2\pi U_{10}} \tag{4.18}$$

where f is the wave frequency. Hsiao and Shemdin's (1983) relation is

$$\frac{B}{f} = 0.12 \frac{\rho_a}{\rho_w} 2\pi (\mu \cos\alpha - 1)^2 \qquad (\frac{U_{10} \cos\alpha}{c}) > 1.0 \tag{4.19}$$

where $\mu = (8/3\pi)\frac{U_{10}}{c}$ and U_{10} stands for the wind speed at height of ten meters.

The analytical and empirical B functions are compared in directionally integrated form. The directionally integrated form of the B function is developed with the aid of the energy transfer equation as described below. The spreading function multiplied by the frequency spectrum can be used to obtain the directional frequency spectrum as

$$E(f, \theta) = E(f)F(\theta) \tag{4.20}$$

Using equation (4.20), for a homogeneous wave field, equation (2.1) without the dissipation and nonlinear interaction terms can be rewritten as

$$\frac{\partial E(f,t)F(\alpha)}{\partial t} = A(U, f, \alpha) + B(u_*, f, \alpha)E(f,t)F(\alpha) \tag{4.21}$$

Integrating equation (4.21) over the parameter α from $-\pi/2$ to $\pi/2$ and taking into consideration that

$$\int_{-\pi/2}^{+\pi/2} F(\alpha)d\alpha = 1$$

equation (4.21) can be written as

$$\frac{\partial E(f,t)}{\partial t} = \int_{-\pi/2}^{+\pi/2} A(U, f, \alpha)d\alpha + \int_{-\pi/2}^{+\pi/2} B(u_*, f, \alpha)E(f,t)F(\alpha)d\alpha \tag{4.22}$$

Letting

$$A'(U,f) = \int_{-\pi/2}^{+\pi/2} A(U,f,\alpha)d\alpha \tag{4.23}$$

and

$$B'(u_*,f) = \int_{-\pi/2}^{+\pi/2} B(u_*,f,\alpha)F(\alpha)d\alpha \tag{4.24}$$

we come to

$$\frac{\partial E(f,t)}{\partial t} = A'(U,f) + B'(u_*,f)E(f) \tag{4.25}$$

Equation (4.25) is the directionally integrated form of the energy transfer equation. It should be observed that it assumes that the spectrum is always centered on the wind direction. In this form of the equation, the B function is in the directionally integrated form (B'). The B function obtained from equation (2.25) is in the directional form. To obtain the directionally integrated form of the B function a spreading function $F(\alpha)$ is required. In the present study the spreading function derived by Cote, et al., (1960), as a function of frequency, direction and wind speed is used. It reads as

$$F(\omega, \alpha, U) = \frac{1}{\pi}[1 + (0.5 + 0.82e^{-\frac{1}{2}(\frac{\omega U}{g})^4}) \cos 2\alpha + 0.32e^{-\frac{1}{2}(\frac{\omega U}{g})^4} \cos 4\alpha]$$

$$for\ -\frac{\pi}{2} < \alpha < \frac{\pi}{2} \tag{4.26}$$

where $\omega = 2\pi f$ and $F(\omega,\alpha,U) = 0$, elsewhere. This is used in equation (4.24) to determine the directionally integrated form of the B function in this study.

The integrals in equation (2.25) are evaluated using two different integration schemes. One scheme uses the Simpson's rule of integration throughout, a fixed step size in the region $kz < 1.0$ ($z < 1.0$) in case of profile 1 (profile 2) and a step size chosen depending on value of the integrand in the region $kz > 1.0$ ($z > 1.0$) in case of profile 1 (profile 2). The other scheme uses Simpson's rule in the region $kz < 1.0$ ($z < 1.0$) in case of profile 1 (profile 2) and Gauss-Laguerre Quadrature in the region $kz > 1.0$ ($z > 1.0$) in case of profile 1 (profile 2). Both the schemes yield identical results. The Gauss-Laguerre scheme is not used throughout the range of integration because it does not follow the strong peak of the integrand close to the origin.

Intially, the B/f values (from equation 2.25) are determined, using the coefficients and constants specified by Phillips (1966), for each mean velocity profile. When mean velocity profile 1 with $A_2 = 10.00$ is used it is seen, in Figure 5 that the B/f values decrease as u_*/c increases. The surface roughness had the functional form shown in equation 3.9. The same trend is observed, when profile 2 is used. In case of profile 2, the wall mixing length is $2.314 \cdot 10^{-4}$ m and the mean velocity at 10 m height is 15.00 m/s. The reason for choosing this wall mixing length is given in the next chapter. The trend seen in Figure 5 is contrary to what is expected. It is thought that the velocity profile is not the reason for the trend. The correlation coefficient M defined in the second chapter, is considered to be a reason for this trend.

According to Phillips (1966), this coefficient is based on Motzfeld's experiments (1937) and theoretical analysis. The coefficient vanishes in inviscid flow. As the wavelength (or wave speed) increases for a given wind speed, the frequency and gradients of the air flow perturbations induced by a wave component decreases. The flow tends to become more and more like a inviscid flow. Hence this correlation should decrease as the wave speed is increased. The above idea is introduced by replacing the coefficient M by $M\,exp(\frac{-0.5\,c}{u_*})$. The B/f values are evaluated with this new coefficient M for the two different mean velocity profiles. When this is done, the two velocity profiles give B/f values which agree more closely with measured values. Figures 6 and 7 show the B/f vs u_*/c curves for profiles 1 and 2 respectively, with the new form for the coefficient M. In figure 6, the three curves correspond to A_2 values of 10.00, 40.00 and 60.00. The wall mixing lengths corresponding to U_{10} values of 10.00 m/s, 15.00 m/s and 20.00 m/s are used in figure 7. Profile 2 gives values comparable to those obtained using the empirical relations of Hsiao and Shemdin (1983), Plant (1982) and Snyder et al. (1981) while the values given by profile 1 are found to be smaller.

The directional behavior of the B function obtained using the velocity profile 2 in equation (2.25) is shown in figure 8. The assumed directional behavior of the B function obtained from the relations of Snyder et al., Plant and Hsiao and Shemdin are shown in Figures 9, 10 and 11 respectively. In all cases profile 2 is used, the mean velocity at 10 m height, wall mixing length and friction velocity being 15 m/s, $2.314 \cdot 10^{-4}$ m and 0.6320 m/s respectively. The directional behavior of the B function obtained from the analytical model, shown in figure 8,

shows significant differences when compared to the other three figures. Figure 10 based on Plant's relation shows a cosα type behavior. Figures 9 and 11 show a different behavior due to the form of imposed limits (refer equations 4.17 and 4.19).

5. Relating the B function to sea state

The procedure used to relate the growth rate to the sea state through the mean velocity profile is discussed in this chapter.

The structure of the layer close to the water surface is closely related to the sea state. The wave induced air flow perturbations depend on the sea state. It is necessary to relate the mean velocity profile to the sea state to understand the interaction at the air-sea interface. Two approaches are used to relate velocity profile 2 to the sea state through the wall mixing length in this chapter. The first approach uses Wu's (1980) relation for drag coefficient while the second approach follows Huang et al.'s (1986) approach to determine the drag coefficient. Results obtained from these approaches are compared later in this chapter. The following paragraph describes the first approach.

Wu's (1980) relation for the drag coefficient $C_d = (u_*/U)^2$, is used for U_{10} greater than 10.00 m/s, to determine the friction velocity as a function of U_{10} only. This

friction velocity is used in profile 2, equation (3.18), to determine the appropriate wall mixing length corresponding to the wind speed assumed at 10 m height. For lower wind speeds an appropriate wall mixing length could not be found using Wu's relation. Wu's relation reads as

$$C_d = (0.8 + 0.065U_{10}) \cdot 10^{-3} \tag{5.1}$$

From the values of the wall mixing length and U_{10} the following relation is assumed.

$$l_o = (6.541 \times 10^{-8}) \cdot U_{10}^{3.006} \tag{5.2}$$

Figure 12 compares the drag coefficient obtained using the equations (3.18) and (5.2), with that obtained from equation (5.1), for the different wind speeds. A wall mixing length of $2.314 \cdot 10^{-4}$ m at U_{10} of 15.00 m/s gives the same drag coefficient as equation (5.1). The C_d values are seen to compare well for the higher wind speeds, as they should. At lower wind speeds there is a significant difference between the two curves as seen in the figure. The drag coefficient obtained from the present model, decreases with the wind speed up to a wind speed of about 5.00 m/s, beyond which point is starts to increase again. Equation (3.18), is derived on the assumption that the sea surface is fully rough. This assumption may not hold good for the lower wind speeds. This may be a possible reason for the difference seen between the two cases and higher values of drag coefficient obtained in the present model, for lower wind speeds.

In order to relate the wall mixing length to the sea state a relation between the sea state and wind speed at 10 m height is required. The significant wave height is considered as representative of the sea state and the DTNSRDC report, Lee, Bales and Sowby (1985), on wave climate in the North Pacific Ocean is used to determine an approximate relation between the significant wave height H_s and U_{10} as below.

$$H_s = 0.022\, U_{10}^{1.85} \tag{5.3}$$

Using relations (5.2) and (5.3) a relation between the wall mixing length and the significant wave height is determined as below.

$$l_o = (3.232 \cdot 10^{-5}) H_s^{1.627} \tag{5.4}$$

It should be understood that in using this relation a wind speed is implied by equation (5.3).

The drag coefficient defined by Wu's relation is a function of wind speed only, whereas other relations like that of Kitaigorodskii (1970) are functions of the significant wave height also. In the second approach, Kitaigorodskii's (1970) parametrization of the roughness length is used . Huang et al. (1986) conducted controlled laboratory experiments to study the influence of wave conditions in determining the drag coefficient. They showed that Kitaigorodskii's (1970) roughness length scale model represented a generalization of the Charnock (1955) and Hsu (1974) models. The details shown in Huang et al. (1986) are followed

to relate the sea state to the roughness length in the present study. A brief outline of the procedure is given below.

The significant wave slope, ζ, is defined as

$$\zeta = \frac{H_{rms}}{\lambda} \tag{5.5}$$

where H_{rms} is the rms wave height and λ is the wavelength corresponding to the frequency at the spectral peak. Kitaigorodskii's (1970) roughness length scale, h_s, is written as

$$h_s = \frac{\pi (m-1)^{0.5}}{2\kappa^2} \zeta \frac{u_*^2}{g} K(\frac{u_*}{c}; m) \tag{5.6}$$

where m is related to ζ as

$$m = \left| \frac{\log(\sqrt{2}\,\pi\zeta)^2}{\log 2} \right| \tag{5.7}$$

and the function K is

$$K = [(\frac{u_*}{2\kappa c})^{m-5} \Gamma(m-1, 2\kappa \frac{c}{u_*})]^{0.5} \tag{5.8}$$

where Γ is the incomplete gamma function. Equation (5.6) does not yield a closed form solution for a general m. However, if m is chosen to be an integer, a closed form solution can be obtained as

$$h_s = [(m-1)!]^{0.5} \left(\frac{1}{X_o}\right)^{\frac{(m-1)}{2}} [1 - \exp(-X_o) \sum_{P=2}^{m} \frac{X_o^{P-2}}{(P-2)!}]^{0.5} H_{rms} \qquad (5.8)$$

where X_o is defined by the following relation.

$$X_o = 2\kappa \frac{c}{u_*} \qquad (5.9)$$

The Jonswap relations (see Hsu, 1985) for a fetch-limited case are used to obtain the value of m for a given U_{10} and fetch, L. They are as below.

$$\frac{gH_s}{U_{10}^2} = 0.0016 \left(\frac{gL}{U_{10}^2}\right)^{1/2} \qquad (5.10)$$

$$\frac{gT_m}{U_{10}} = 0.2857 \left(\frac{gL}{U_{10}^2}\right)^{1/3} \qquad (5.11)$$

where T_m is the period corresponding to the spectral peak. Using equations (5.10) , (5.11) and the deep water relation $\lambda = \frac{g}{2\pi} T_m^2$ the following equation is obtained.

$$\frac{H_s}{\lambda} = 0.1232 \left(\frac{U_{10}^2}{gL}\right)^{1/6} \qquad (5.12)$$

Making use of equation (5.5) and $H_{rms} = \frac{H_s}{1.41}$ we get

$$\zeta = 0.0873 \left(\frac{U_{10}^2}{gL}\right)^{1/6} \qquad (5.13)$$

from which the value of m can be found using equation (5.7). The value of m increases from about 5 to 7 with the sea state development. A value of m = 7, for which $\zeta = 0.01988$, corresponds roughly to a fully developed sea. The Pierson-Moskowitz (1964) spectrum gives a m value of 7.280.

The mean relationship between surface roughness, z_o, and the roughness length scale, h_s, is taken as

$$z_o = \frac{h_s}{20} \tag{5.14}$$

and the logarithmic velocity profile is used to find the drag coefficient as in Huang et al. (1986).

$$C_d = \left(\frac{\kappa}{\ln \frac{z}{z_0}}\right)^2 \tag{5.15}$$

The wind velocity is specified at z = 10.00 m. The surface roughness is determined in terms of the friction velocity, u_*, from equations (5.8) and (5.14) for a given wind speed and sea state, specified by a significant wave height. The drag coefficient is determined using equation (5.15) by iterating for the friction velocity. The friction velocity determined is used in profile 2 (equation 3.18) to determine the corresponding wall mixing length.

Due to the nature of the relations, in the first approach we have one wall mixing length and significant wave height corresponding to a U_{10} and an implied relation

between H_s and U_{10} while in the second approach we can have a range of wall mixing lengths and significant wave heights corresponding to a U_{10} . The drag coefficients and wall mixing lengths obtained in the second approach are found to be comparable to those obtained in the first approach only for a fairly well developed sea (m = 7). Table 1. compares the wall mixing lengths and drag coefficients obtained using the second approach, for m = 7, and the first approach for different wind speeds. The significant wave heights shown in the table are found using equation (5.3). The wall mixing lengths and drag coefficients obtained for different values of m in the second approach are shown in table 2. It is seen from the table that the wall mixing length decreases with the development of sea state.

Using one of the above approaches the friction velocity and wall mixing length are found. The mean velocity profile 2 is then used in equation (2.25) to determine the B/f values. Figure 13 compares the B function obtained from the present analytical model, using velocity profile 2 based on the first approach, with the growth rate obtained from the empirical relations based on pressure measurements. Figure 14 does the same except that velocity profile 2 is based on the second approach. In both cases the wind speed at 10 m height and significant wave height are 15.00 m/s and 3.29 m respectively. This compares to a fully developed significant wave height (from Pierson-Moskowitz spectrum) of 5.5 m. The B function values obtained using both the approaches are seen to compare with the B function values based on the pressure measurements. Figure 15, based on the second approach shows how the B function varies with the sea state. The

wind speed at 10 m height is 15.00 m/s for all the cases shown in the figure. As the development of sea state advances, the growth rate function is found to increase as seen in the figure.

6. Conclusions and Recommendations

An analytical model for the growth rate, which gives results comparable to those of the empirical relations and a procedure to relate the sea state to the mean wind velocity profile and through it to the growth rate, has been developed. An appropriate mean wind velocity profile over the sea surface has been determined. The profile, based on a mixing length formulation, is related to the sea state through the wall mixing length. The growth rate is then related to the sea state through the mean velocity profile. A correction to the correlation coefficient M, in the analytical model of Phillips (1966), is found necessary to obtain growth rates comparable to those given by the empirical relations based on pressure measurements. The directional behavior of the B function obtained in the present model is found to differ from the directional behavior of the B functions based on the empirical relations.

The ambiguities in definition of the functional form of sea surface roughness for smooth and rough surfaces should be resolved. Extension of the mean velocity

profile based on the mixing length formulation to smooth sea surfaces can be attempted. The relationship between the drag coefficient and the sea state with respect to time should be investigated in detail by conducting experiments in the laboratory and field since it is very important for the determination of the growth rate.

References

Barnett, T.P. and J.C. Wilkerson, "On the interpretation of fetch-limited wave spectra as measured by an airborne sea-swell recorder ", U.S. Naval Oceanographic Office, TR-191, 60 pp, 1966.

Bryant, P.J., Ph.D. Dissertation, University of Cambridge, 1966.

Coté et al., "The directional spectrum of a wind generated sea as determined from data obtained by the Stereo Wave Observation Project", Meteor. Pap., Vol. 2, No. 6, 88 pp., New York University Press, NY, (1960).

Charnock, H., "Wind stress on water surface. ", Quart. J. Roy. Meteor. Soc., 81, 639-640, 1955.

Dobson, F.W., "Measurements of atmospheric pressure on wind-generated sea waves", J. Fluid Mech., 48, 91-127, 1971.

Elliot, J.A., "Microscale pressure fluctuations near waves being generated by the wind ", J. Fluid Mech., 54, 427-448, 1972.

Granville, S.P., "Mixing length formulations for turbulent boundary layers over arbitrarily rough surfaces ", J. Ship Res., 29, 223-233, 1985.

Hasselmann, K., "Grundgleichungen der Seegangsvorhersage ", Schiffstechnik, 7, 191-195, 1960.

Hasselmann, K., "On the nonlinear energy transfer in a gravity-wave spectrum", Part 1, General theory, J. Fluid Mech., 12, 481-500, 1961.

Hasselmann, K., et al., "Measurements of wind-wave growth and swell decay during the Joint North Sea Wave Project (JONSWAP) ", Dtsch. Hydrogr. Z. Suppl. A, 12, 1-95, 1973.

Hsu, S.A., "A dynamic roughness equation and its application to wind stress determination at the air-sea interface ", J. Phys. Oceanogr., 4, 116-120, 1974.

Hsu, S.A., "A mechanism for the increase of wind stress (drag) coefficient with wind speed over water surfaces: A parametric model", J. Phys. Oceanogr., 16, 144-149, 1985.

Huang, N.E., L.F. Bliven, S.R. Long and P.S. DeLeonibus, "A study of the relationship among wind speed, sea state, and the drag coefficient for a developing wave field", J. Geophys. Res., 91, 7733-7742, 1986.

Hsiao, S.V. and O.H. Shemdin, "Measurements of wind velocity and pressure with a wave follower during MARSEN ", J. Geophys. Res., 88, 9841-9849, 1983.

Inoue, T., "On the growth of the spectrum of a wind generated sea according to a modified Miles-Phillips mechanism and its application to wave forecasting", TR-67-5, Geophysical Science Laboratory Report, NY University, School of Engineering and Science, 1967.

Jeffreys, H., "On the formation of water waves by wind", Proc. Roy. Soc., Series A, 107, 189-206, 1925.

Kawai, S., "Generation of intial wavelets by instability of a coupled shear flow and their evolution to wind waves", J. Fluid Mech., 93, 661-703, 1979.

Kinsman, B., Wind waves, Prentice-Hall, 1965.

Kitaigorodskii, S.A., "The physics of air-sea interaction", Gidrometeorologicheskoe Izadatel'stvo, Leningrad, USSR, 1970. (English translation, Israel program for scientific translations, Jerusalem, 1973.).

Komen, G.T., S. Hasselman and K. Hasselman, "On the existence of a fully developed wind-sea spectrum ", J. Phys. Oceanogr., 14, 1271-1285, 1984.

Kondo, J., "Air-sea bulk transfer coefficients in diabatic conditions", Bound. Layer Meteor., 9, 91-112, 1975.

Kwon, S.H., "Directional growth of wind generated waves", Ph.D. Dissertation, Virginia Polytechnic Institute and State University., 1986.

Larson, T.R. and J.W. Wright, "Wind-generated gravity-capillary waves: Laboratory measurements of temporal growth rates using microwave backscatter", J. Fluid Mech., 70, 417-436, 1975.

Lee, W.T., S.L. Bales and S.E. Sowby, "Standardized wind and wave environments for North Pacific ocean areas", DTNSRDC Report, 1985.

Liu, W.T. and J.A. Businger, "Temperature profile in the molecular sublayer near the interface of a fluid in turbulent motion", Geophys. Res. Lett., 2, 403-404, 1975.

Liu, W.T., K.B. Katsaros and J.A. Businger, "Bulk parametrization of air-sea exchanges of heat and water vapor including the molecular constraints at the interface", J. Atmos. Sci., 36, 1722-1734, 1979.

McDonald, B.E., "On the stress-shear relation near a turbulent air-sea interface", NORDA Tech. Note 181,1982.

Miles, J.W., "On the generation of surface waves by shear flow", Part 1, J. Fluid Mech., 3, 185-204, 1957; Part 2, J. Fluid Mech., 6, 568-582, 1959; Part 3, J. Fluid Mech., 6, 583-598, 1959; Part 4, J. Fluid Mech., 7, 469-478, 1960.

Moskowitz, L., W.J. Pierson and E. Mehr, "Wave spectra estimated from wave records obtained by the OWS 'Weather Explorer' and the OWS 'Weather Reporter'", Parts I, II, and III, Tech. Reports, New York University, School of Engineering and Science, Dept. of Meteor. and Oceanography, 1962,1963 and 1965.

Motzfeld, H., "Die turbulente strömung an welligen wanden", Z. agnew Math. Mech. 17, 193-212, 1937.

Neu, W.L. and S.H. Kwon, "A directional growth mechanism for SOWM-Type wave models", VPI-AOE-150 Report, Aerospace and Ocean Engineering Dept., Virginia Polytechnic Institute and State University, 1985.

Phillips, O.M., "On the generation of surface waves by turbulent wind", J. Fluid Mech., 2, 417-445, 1957.

Phillips, O.M., The dynamics of the upper ocean, Cambridge University Press, NY, 1966.

Pierson, W.J., "The spectral ocean wave model, a northern hemisphere computer model for specifying and forecasting ocean wave spectra", DTNSRDC Report, 1982.

Pierson, W.J. and L.I. Moskowitz, "A proposed form for fully developed seas based on the similarity theory of S.A. Kitaigorodskii ", J. Geophys. Res., 69 (24), 5181-5203, 1964.

Plant, W.J., "On the steady-state energy balance of short gravity wave systems ", J. Phys. Oceanogr., 10, 1340-1352, 1980.

Plant, W.J., "A relationship between wind stress and wave slope", J. Geophys. Res., 87, 1961-1967, 1982.

Rotta, J.C., "Das in wandnähe gültige geschwindigkeitsgestez turbulenter strömungen", Ingenieur-Archiv, 18, 277-280, 1950.

Schetz, J.A., Foundations of boundary layer theory for momentum, heat and mass transfer, Prentice-Hall, 1984.

Shemdin, O.H. and E.Y. Hsu, "Direct measurement of aerodynamic pressure above a simple progressive gravity wave", J. Fluid Mech., 30, 403-416, 1967.

Shemdin, O.H., "Instantaneous velocity and pressure measurements above propagating waves", Tech. Rep. 4, Coastal and Oceanogr. Eng., Univ. of Florida, Gainesville, 1969.

Snyder, R.L. and C.S. Cox, "A field study of the wind generation of ocean waves", J. Mar. Res., 24, 141-178, 1966.

Snyder, R.L., "A field study of wave-induced pressure fluctuations above surface gravity waves", J. Mar. Res., 32(3), 497-531, 1974.

Snyder, R.L., F.W. Dobson, J.A. Elliott and R.B. Long, "Array measurements of atmospheric pressure fluctuations above surface gravity waves", J. Fluid Mech., 102, 1-59, 1981.

SWAMP group, Ocean wave modeling, Plenum Press, NY and London, 1985.

Takeda, A., "Wind profiles over sea waves", J. Ocean Soc., Japan, 19, 16-22, 1963.

Wu, J., "Laboratory studies of wind wave interactions", J. Fluid Mech., 34, Part 1, 91-111, 1968.

Wu, H.Y., E.Y. Hsu and R.L. Street, "The energy transfer due to air-input, non-linear wave-wave interaction and white cap dissipation associated with wind-generated waves ", Tech. Rep. 207, pp. 1-158, Stanford Univ., Stanford, Calif., 1977.

Wu, H.Y., E.Y. Hsu and R.L. Street, "Experimental study of nonlinear wave-wave interaction and white-cap dissipation of wind-generated waves ", Dyn. Atmos. Oceans, 3, 55-78, 1979.

Wu, J., "Wind-stress coefficients over sea surface near neutral conditions", J. Phys. Oceanogr., 10, 727-740, 1980.

Table 1. Comparison of wall mixing lengths and drag coefficients.

		First approach		Second approach m = 7	
U_{10} m/s	H_s m	$C_d \cdot 10^3$	$l_o \cdot 10^4$ m	$C_d \cdot 10^3$	$l_o \cdot 10^4$ m
10.00	1.557	1.450	0.6541	1.400	0.4965
15.00	3.297	1.775	2.3140	1.761	2.2220
20.00	5.614	2.099	5.2539	2.127	5.5620

Table 2. Wall mixing lengths and drag coefficients for different m's.

U_{10} m/s	m	H_s m	$C_d \cdot 10^3$	$l_o \cdot 10^4$ m
10.00	5	0.171	2.150	5.820
10.00	6	0.485	1.966	3.775
10.00	7	1.360	1.425	0.565
15.00	5	0.386	3.090	25.554
15.00	6	1.091	2.525	11.620
15.00	7	3.080	1.778	2.338
20.00	5	0.687	3.247	30.070
20.00	6	1.940	3.092	25.600
20.00	7	5.476	2.135	5.652

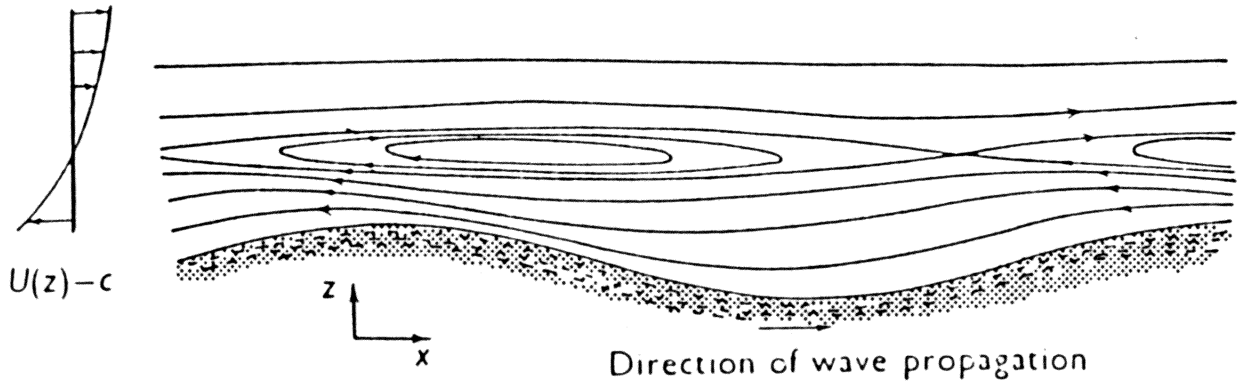

Figure 1. Co-ordinate system and mean streamlines in frame of reference moving with the wave (from Phillips, 1966).

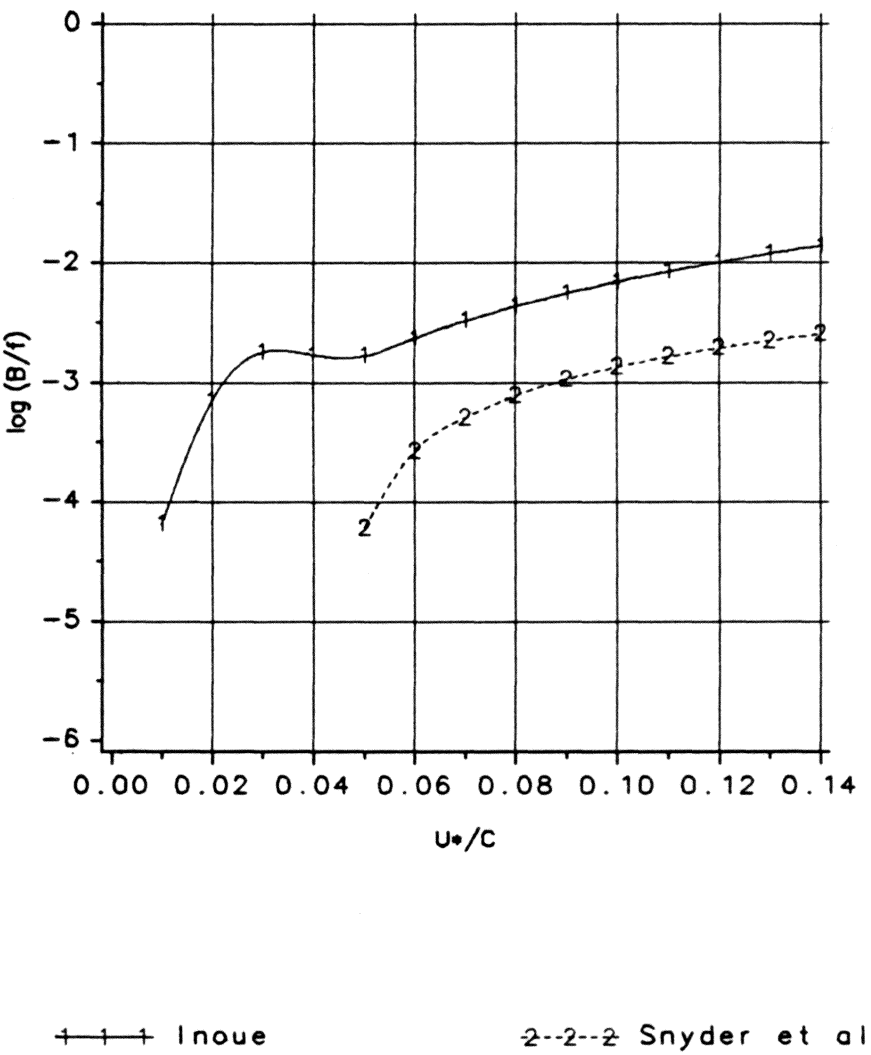

Figure 2. B function from wave growth and pressure measurements.

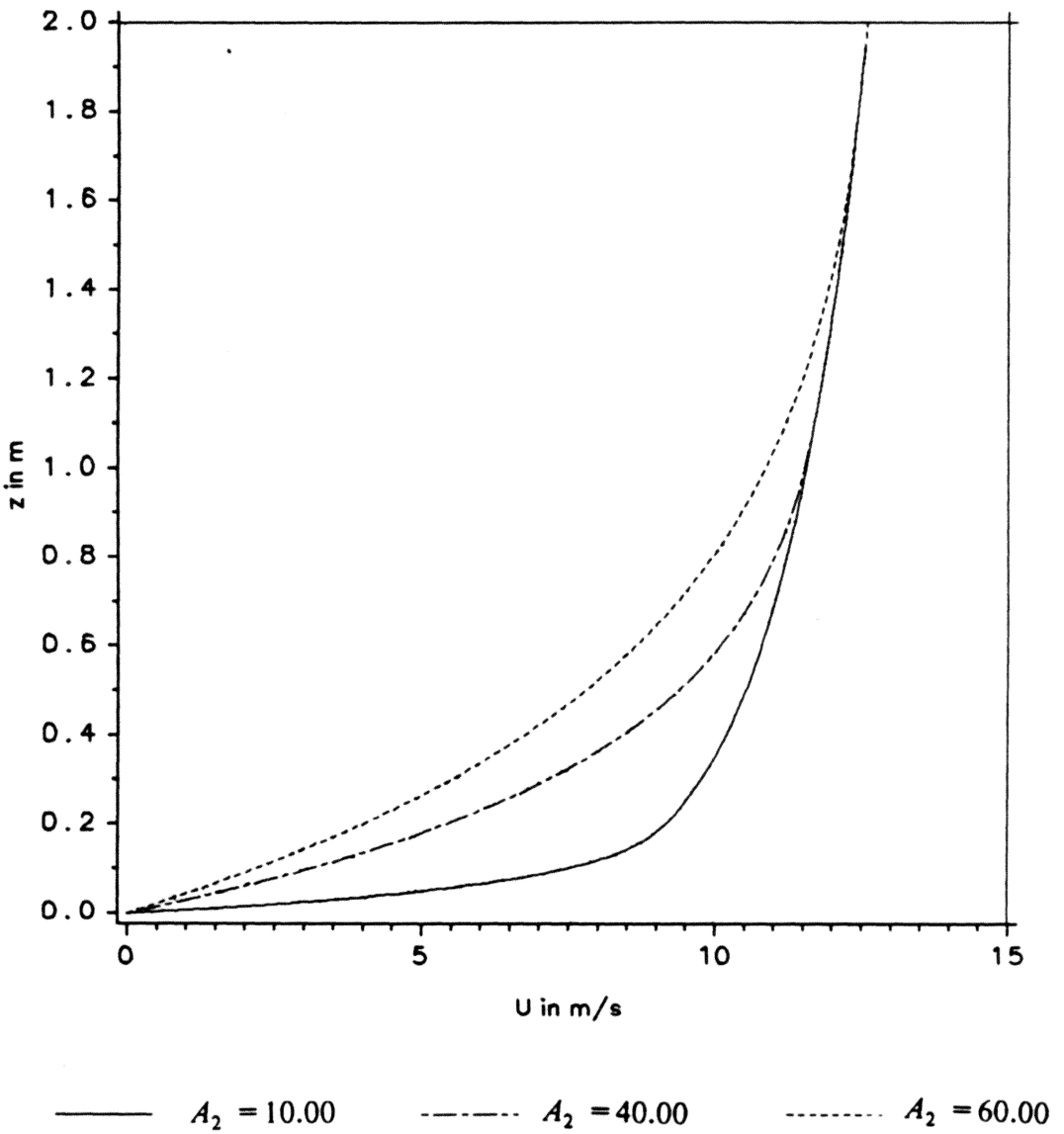

Figure 3. Mean velocity profile 1 for different A_2 values.

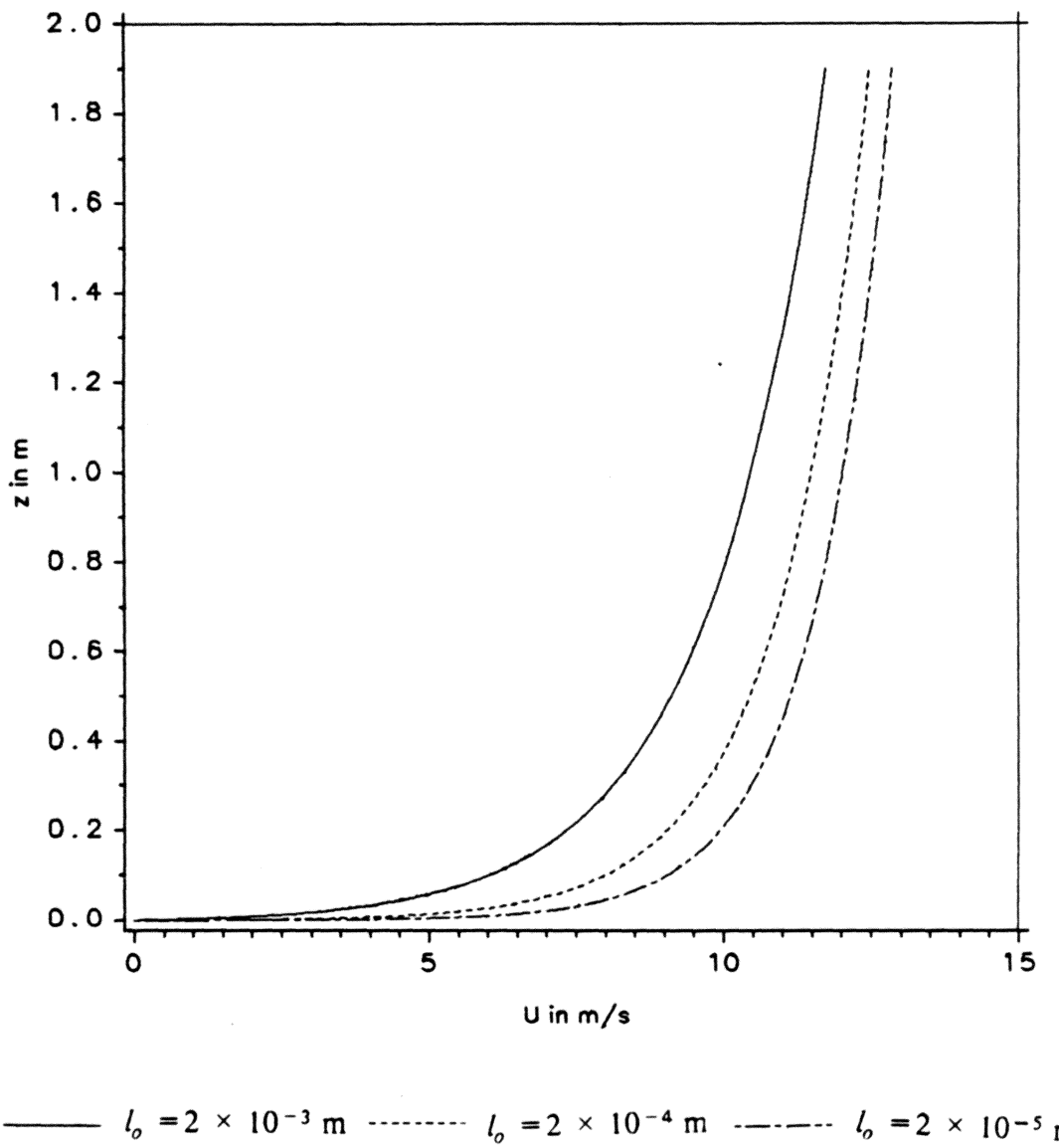

Figure 4. Mean velocity profile 2 for different wall mixing lengths.

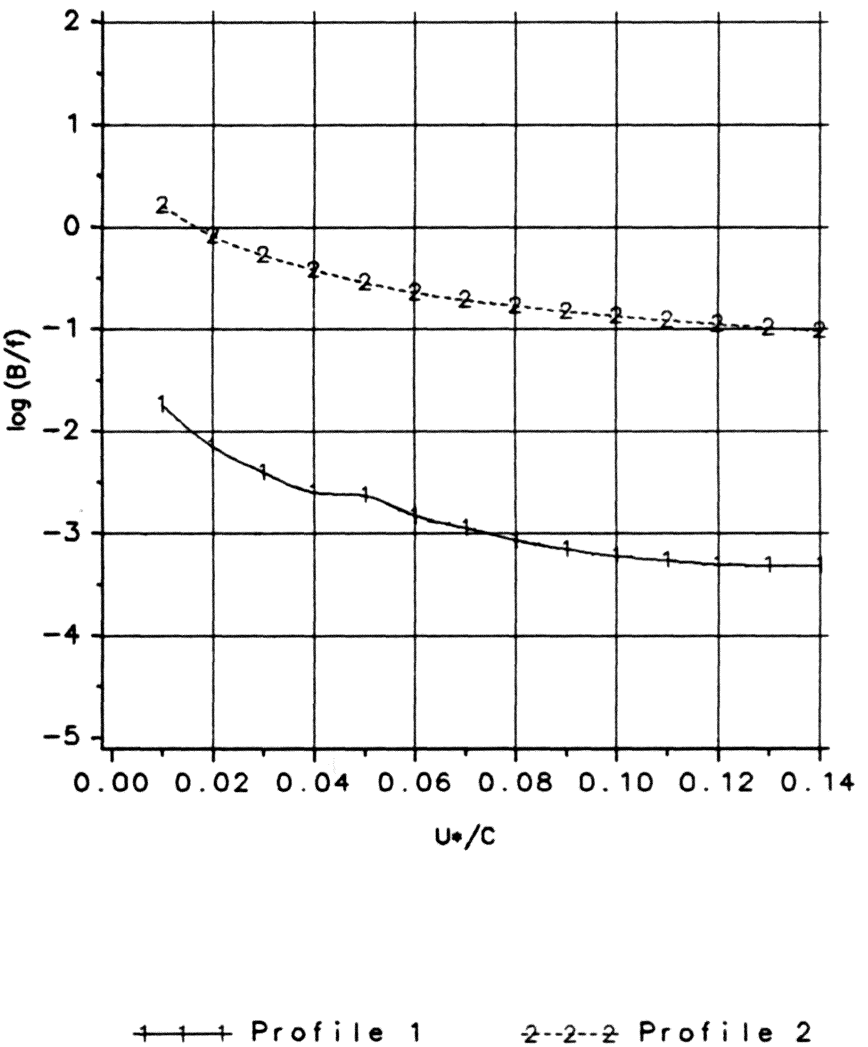

Figure 5. B function from analytical model using Phillips coefficients.

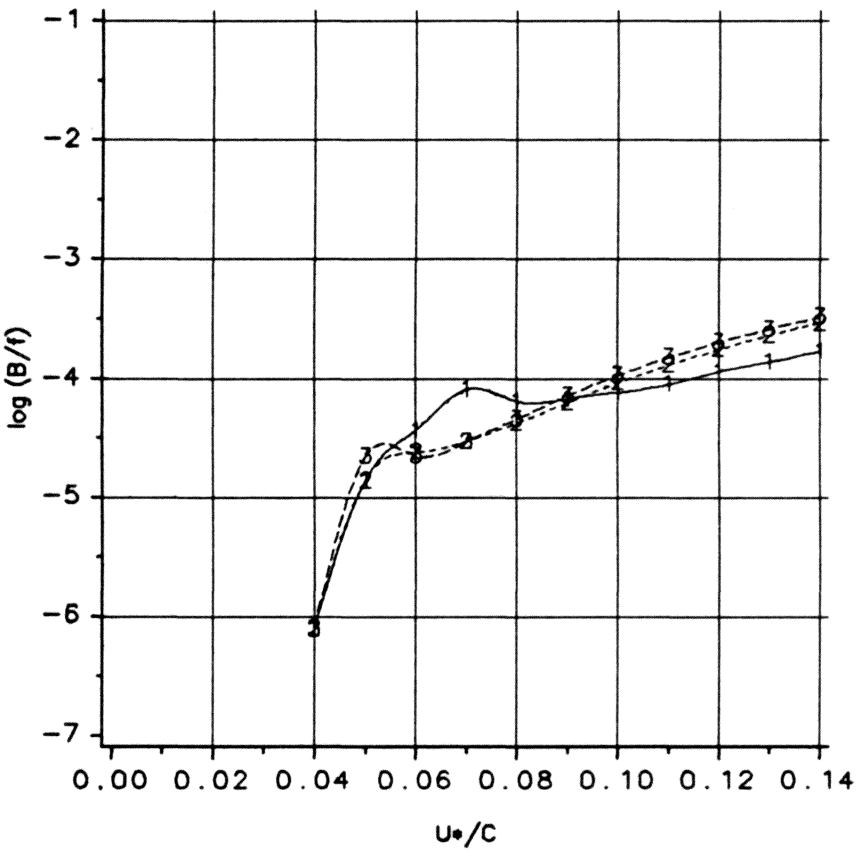

1—1—1 $A_2 = 10.00$ 2--2--2 $A_2 = 40.00$ 3–3–3 $A_2 = 60.00$

Figure 6. B function from analytical model using velocity profile 1 with new coefficient M.

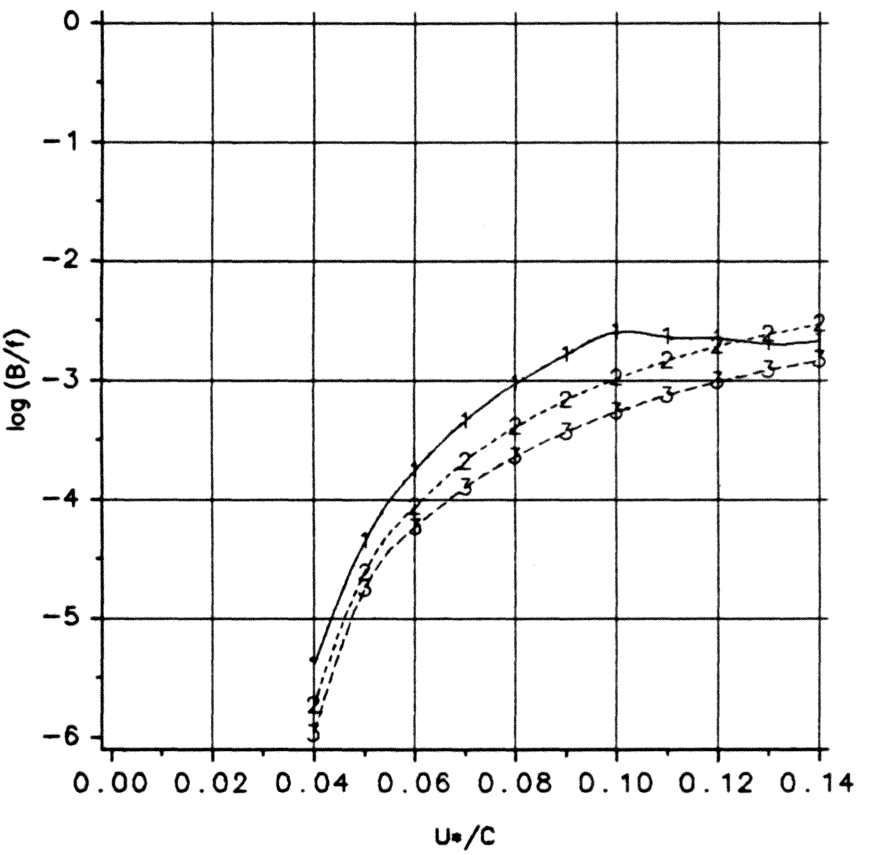

1 1 1 $l_o = 6.541 \times 10^{-5}$ m 2 2 2 $l_o = 2.314 \times 10^{-4}$ m

3 3 3 $l_o = 5.254 \times 10^{-4}$ m

Figure 7. B function from analytical model using velocity profile 2 with new coefficient M.

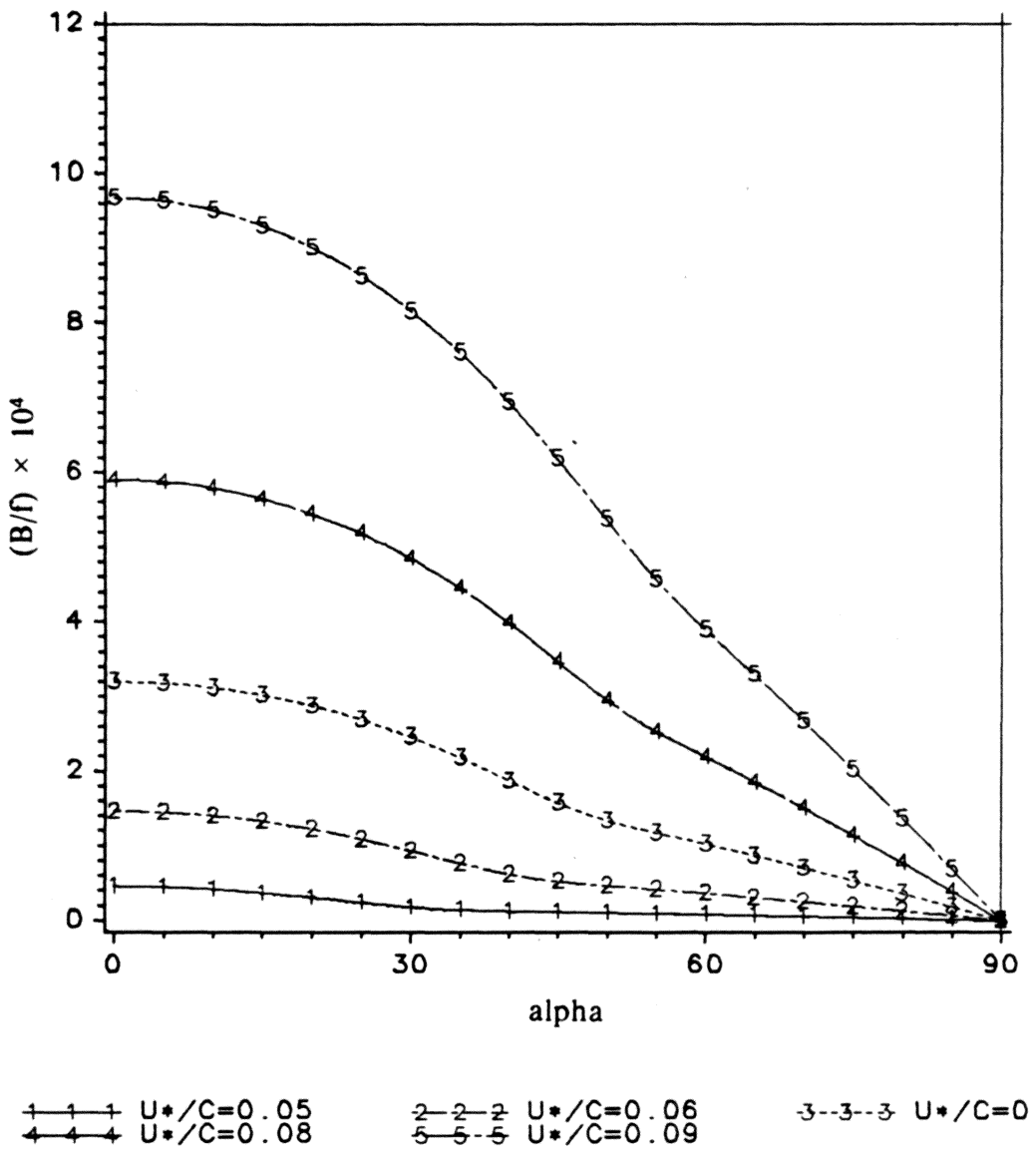

Figure 8. Directional behavior of the B function from analytical model using velocity profile 2.

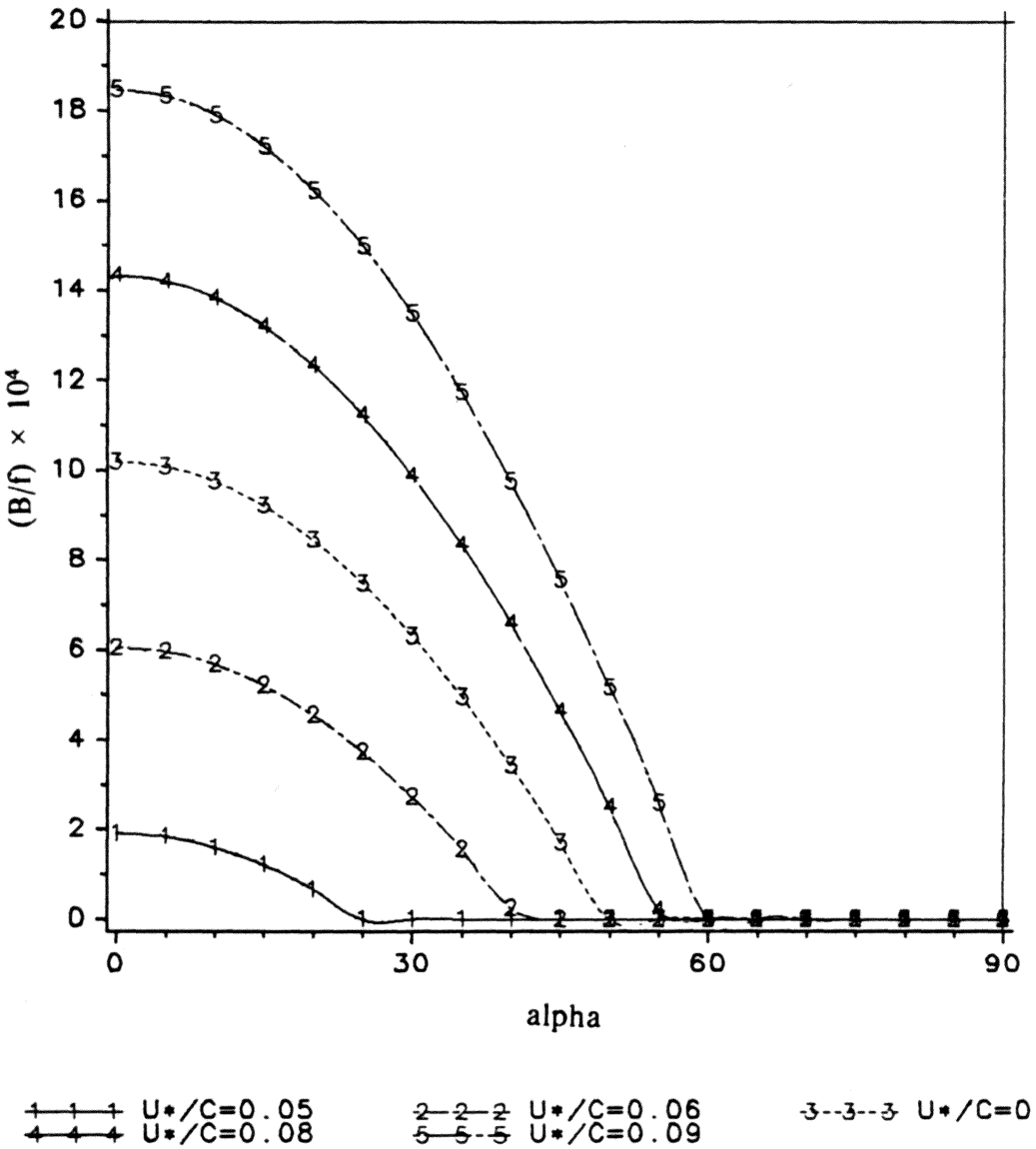

Figure 9. Directional behavior of the B function from Snyder et al.'s empirical relation.

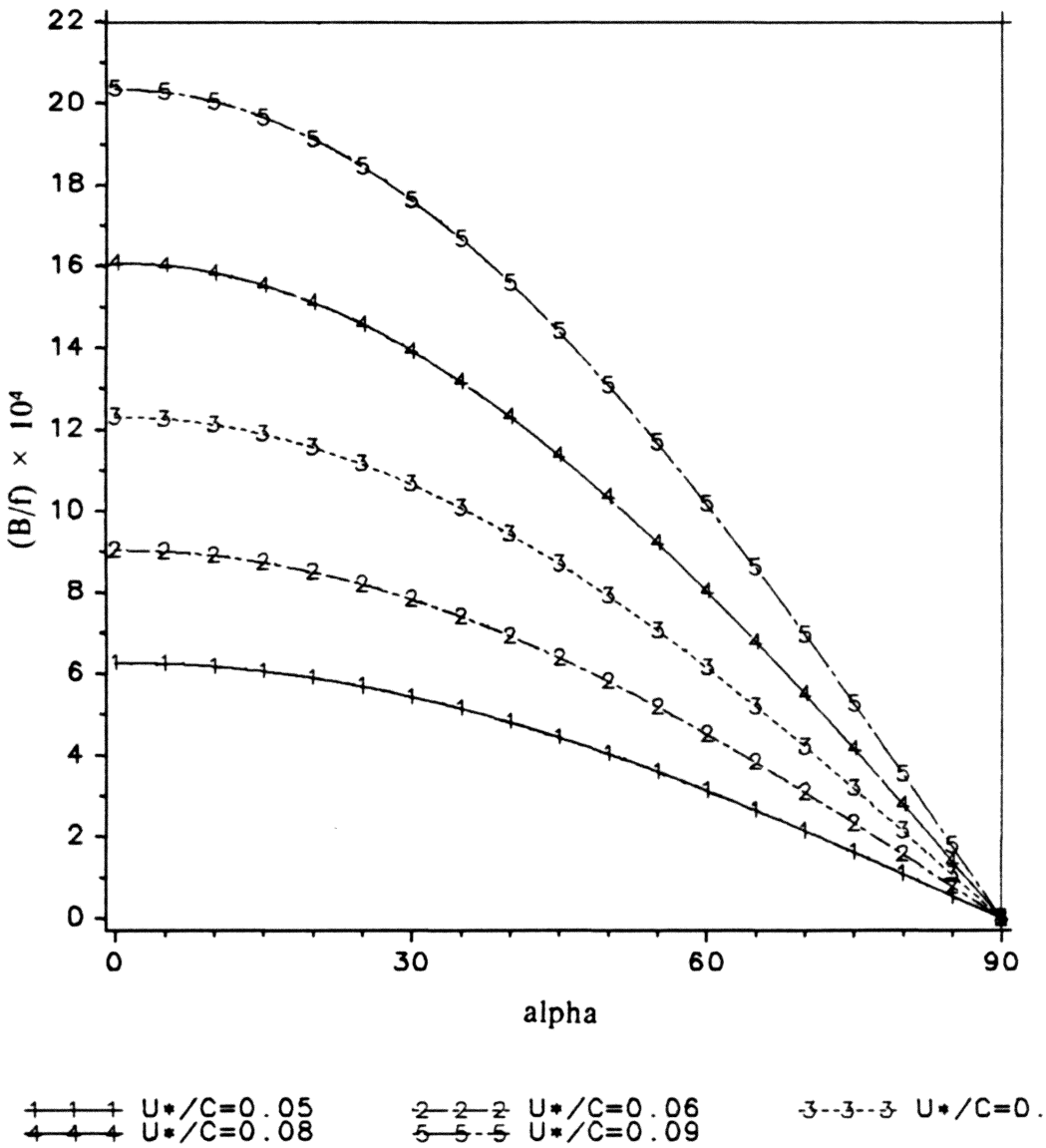

Figure 10. Directional behavior of the B function from Plant's empirical relation.

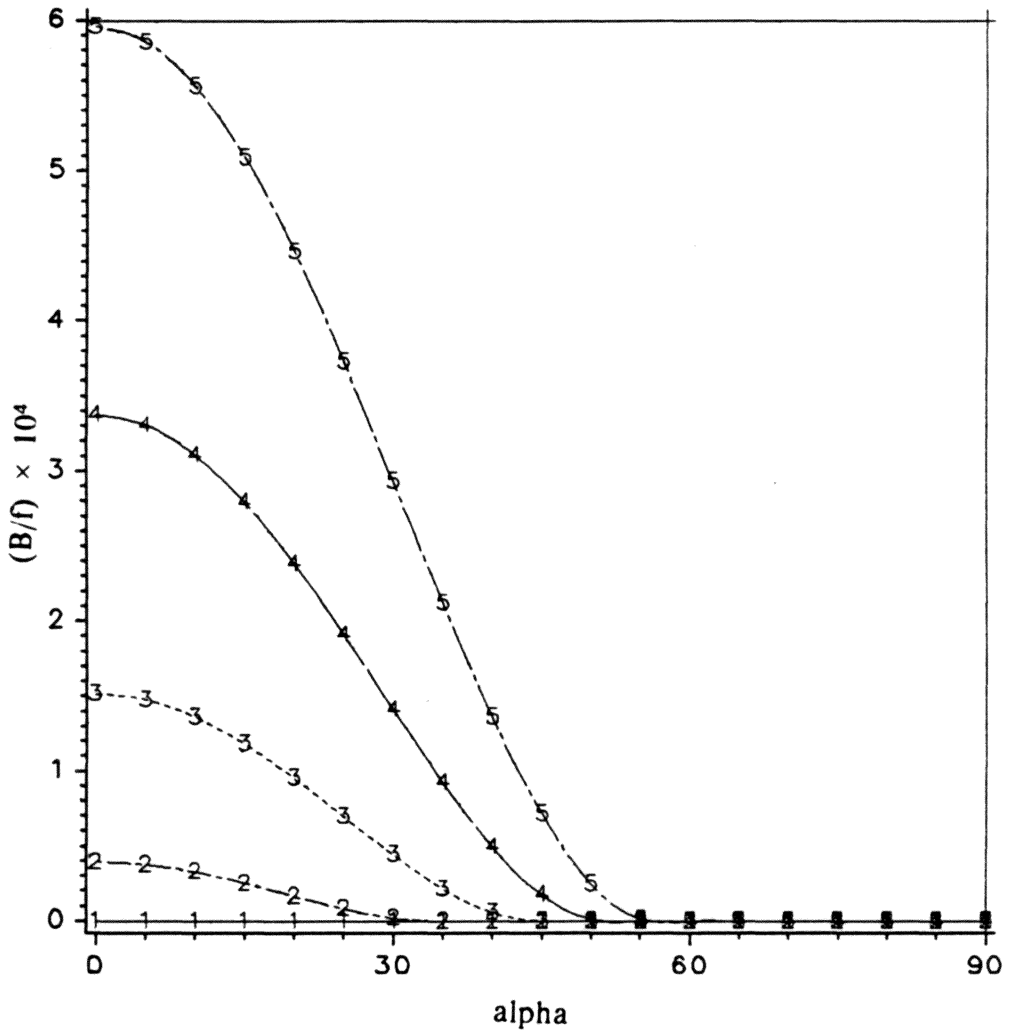

Figure 11. Directional behavior of the B function from Hsiao and Shemdin's empirical relation.

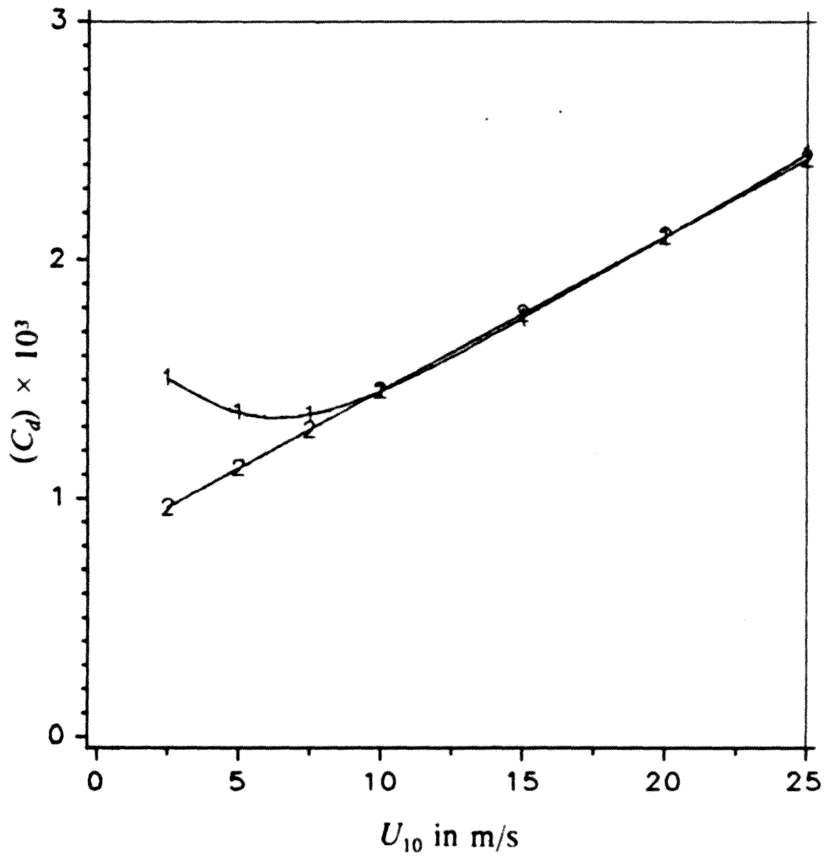

Figure 12. Comparison of drag coefficient from Wu's relation and first approach.

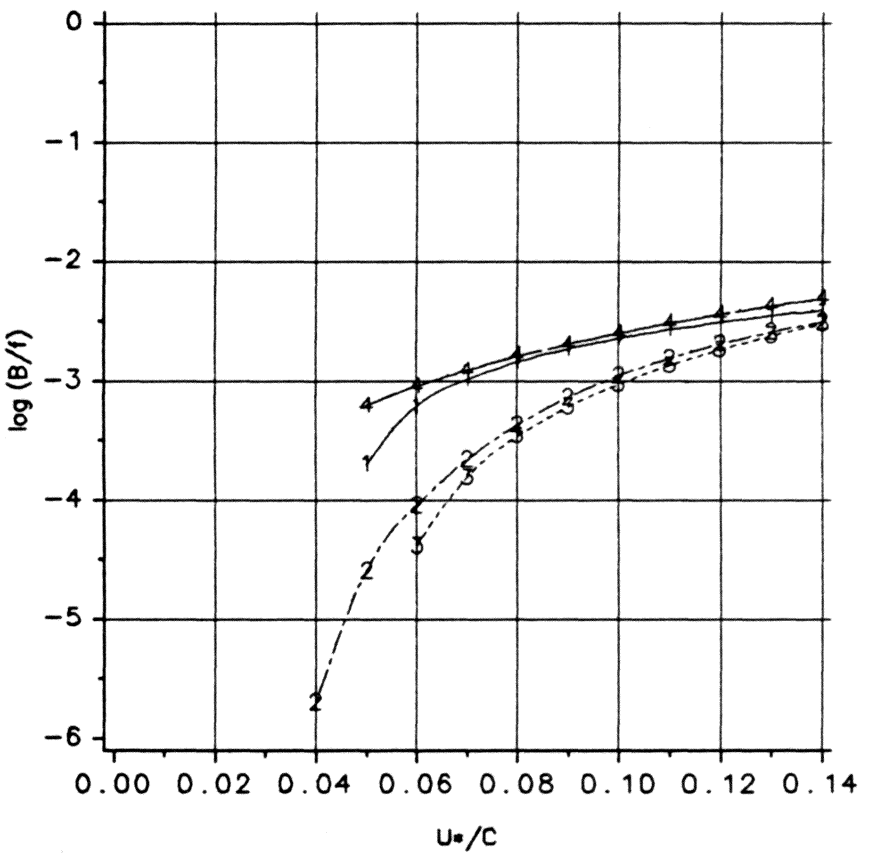

Figure 13. Comparison of the B function from analytical model (using first approach) with the B function from empirical relations.

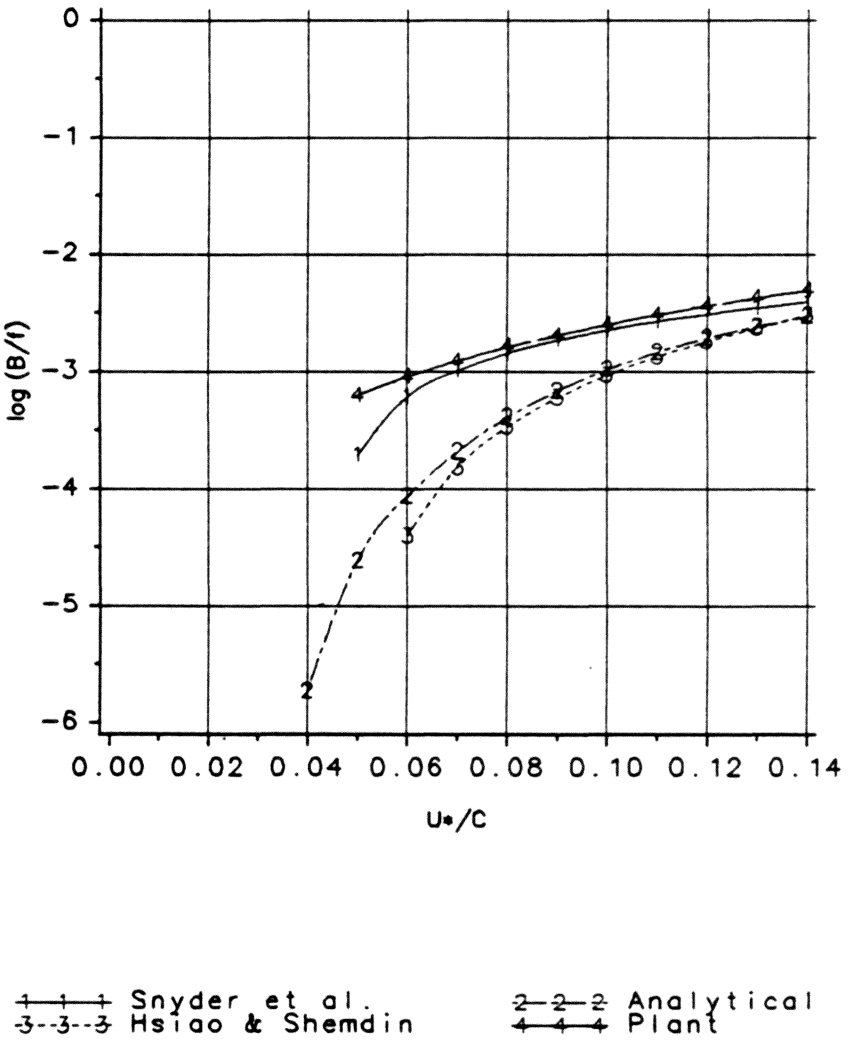

Figure 14. Comparison of the B function from analytical model (using second approach) with the B function from empirical relations.

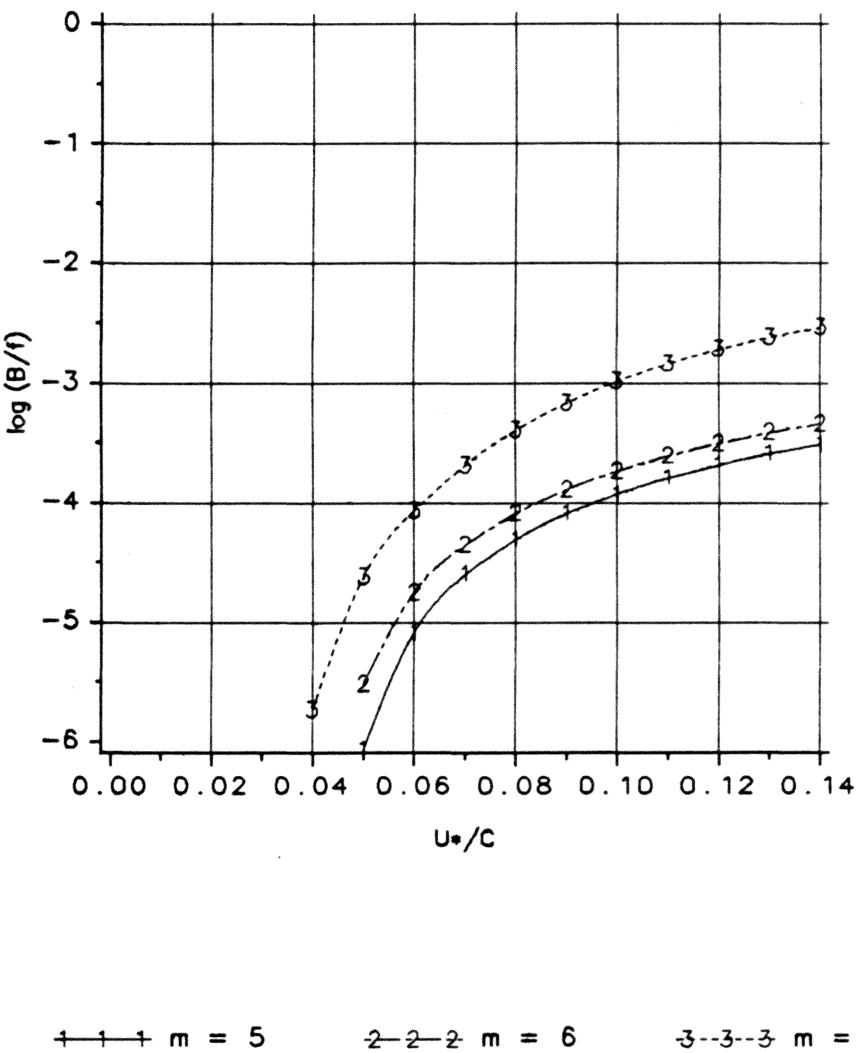

Figure 15. B function from analytical model (using second approach) for different sea states.

Appendix

The sea surface displacement $\eta(\vec{x}, t)$ can be expressed in terms of its generalized Fourier transform $D(\vec{k})$.

$$\eta(\vec{x}, t) = \int D(\vec{k}) e^{i\vec{k} \cdot (\vec{x} - \vec{c}\, t)} d\vec{k} \tag{1.0}$$

where the integration is done over wave number space $(\vec{k})$. Using equation (1.0) we can get the following relation.

$$\eta^*(\vec{x}, t) = \int D^*(\vec{k}_1) e^{-i\vec{k}_1 \cdot (\vec{x} - \vec{c}\, t)} d\vec{k}_1 \tag{1.1}$$

where superscript * indicates complex conjugate.

The covariance function, $H(\vec{x}, t)$, for the sea surface is defined as

$$H(\vec{x}, t) = \overline{\eta(\vec{x}, t)\, \eta^*(\vec{x}, t)} \tag{1.2}$$

where the bar means a space average over x and y directions at an instant t. The following equation is obtained using equations (1.0), (1.1) and (1.2).

$$H(\vec{x}, t) = \int\int \overline{D(\vec{k})\, D^{*}(\vec{k}_1)}\, e^{i\vec{k}\cdot(\vec{x} - \vec{c}\,t)}\, e^{-i\vec{k}_1\cdot(\vec{x} - \vec{c}\,t)} d\vec{k}\, d\vec{k}_1 \tag{1.3}$$

Letting $\vec{k}_{11} = \vec{k} - \vec{k}_1$ equation (1.3) can be written as below.

$$H(\vec{x}, t) = \int\int \overline{D(\vec{k})\, D^{*}(\vec{k} - \vec{k}_{11})}\, e^{i\vec{k}_{11}\cdot(\vec{x})}\, e^{-i\vec{k}_{11}\cdot(\vec{c}\,t)} d\vec{k}\, d\vec{k}_{11}. \tag{1.4}$$

The wave number spectrum $E(\vec{x}, \vec{k}, t)$ is related to the covariance function by the following equation.

$$H(\vec{x}, t) = \int E(\vec{x}, \vec{k}, t) d\vec{k} \tag{1.5}$$

From equations (1.4) and (1.5) we get

$$E(\vec{x}, \vec{k}, t) = \int \overline{D(\vec{k})\, D^{*}(\vec{k} - \vec{k}_{11})}\, e^{i\vec{k}_{11}\cdot(\vec{x} - \vec{c}\,t)} d\vec{k}_{11} \tag{1.6}$$

whose inverse is

$$\overline{D(\vec{k})\, D^{*}(\vec{k} - \vec{k}_{11})} = (2\pi)^{-2} \int E(\vec{x}, \vec{k}, t)\, e^{-i\vec{k}_{11}\cdot(\vec{x} - \vec{c}\,t)}\, d(\vec{x} - \vec{c}\,t) \tag{1.7}$$

The Dirac delta function can be expressed in terms of a fourier transform as below.

$$\delta(\vec{k}) = (2\pi)^{-2} \int e^{-i\vec{k}\cdot\vec{x}}\, d\vec{x} \tag{1.8}$$

If the sea is considered to be a homogeneous and stationary random process, then the wave number spectrum must be independent of space, $\vec{x}$ and time, t. The left hand side of equation (1.7) should have the product $\overline{D(\vec{k})\, D^*(\vec{k} - \vec{k}_{11})}$ in the form of a Dirac delta function with the only contribution to the integral occurring at $\vec{k} - \vec{k}_1 = 0$. Using equation (1.8), this can be expressed by

$$\overline{D(\vec{k})\, D^*(\vec{k} - \vec{k}_{11})} = \delta(\vec{k} - \vec{k}_1) E(\vec{k}) \tag{1.9}$$

Contributions to the covariance in equation (1.9) arise from the same wave numbers. $E(\vec{k})$ is the two dimensional wave spectrum for a spatially homogeneous and stationary wave field.

The vita has been removed from the scanned document